Open-loop optimal control of batch chromatographic separation processes using direct collocation

Holmqvist, Anders; Magnusson, Fredrik

Published in:
Journal of Process Control

DOI:
10.1016/j.jprocont.2016.08.002

2016

Document Version:
Peer reviewed version (aka post-print)

Journal of Process Control 46 (2016) 55–74

Contents lists available at ScienceDirect

Journal of Process Control

journal homepage: www.elsevier.com/locate/jprocont

Open-loop optimal control of batch chromatographic separation processes using direct collocation

A. Holmqvist [a,*], F. Magnusson [b]

[a] Department of Chemical Engineering, Lund University, P.O. Box 124, SE-221 00 Lund, Sweden
[b] Department of Automatic Control, Lund University, P.O. Box 118, SE-221 00 Lund, Sweden

ARTICLE INFO

Article history:
Received 4 September 2015
Received in revised form 14 June 2016
Accepted 17 August 2016

Keywords:
Batch chromatography
PDE-constrained dynamic optimization
Optimal control
Nonlinear programming
Collocation
Algorithmic differentiation

ABSTRACT

This contribution presents a novel model-based methodology for open-loop optimal control of batch high-pressure liquid chromatographic (HPLC) separation processes. The framework allows for simultaneous optimization of target component recovery yield and production rate with respect to a parameterization of the input elution trajectory and fractionating interval endpoints. The proposed methodology implies formulating and solving a large-scale dynamic optimization problem (DOP) constrained by partial differential equations (PDEs) governing the multi-component system dynamics. It is based on a simultaneous method where both the control and state variables are fully discretized in the temporal domain, using direct local collocation on finite elements, and the state variables are discretized in the spatial domain, using an adaptive finite volume weighted essentially non-oscillatory (WENO) scheme. The direct transcription of the DOP described by Modelica, and its extension Optimica, code into a sparse nonlinear programming problem (NLP) is thoroughly presented. The NLP was subsequently solved using CasADi's (**C**omputer **al**gebra **s**ystem with **A**utomatic **Di**fferentiation) interface to the primal-dual interior point method IPOPT. The advantages of the open-loop optimal control strategy are highlighted through the solution of a challenging ternary complex mixture separation problem of human insulin analogs, with the intermediately eluting component as the target, for a hydrophobic interaction chromatography system. Moreover, the high intercorrelation between the shape of the optimal elution trajectories and the fractionation interval endpoints is thoroughly investigated. It is also demonstrated that the direct transcription methodology enabled accurate and efficient computation of optimal cyclic-steady-state solutions, which govern that state and control variables conform to periodicity constraints imposed on column regeneration and re-equilibration. By these means, the generic methods and tools developed here are applicable to continuous chromatographic separation technologies, including the continuous simulated moving bed (SMB) and the multicolumn counter-current solvent gradient purification (MCSGP) process.

1. Introduction

Optimal isolation of a high-purity target component from a multi-component mixture is of significant importance in the pharmaceutical and biochemical industries [1]. In the clinical or commercial-scale manufacturing of human therapeutic proteins, high-pressure liquid chromatography (HPLC) is an essential process operation to achieve the high purity requirements for biopharmaceutical drugs [2,3]. Especially, in the production processes from inclusion bodies, impurities closely related to the product, both in terms of size and charge, are created as byproducts of the refold process. The removal of such product related impurities are usually challenging even for high resolution (analytical) chromatography separation with high performance resins and optimized elution mode [4]. Additionally, performing this type of separation in preparative chromatography for commercial production adds increased complexity. To improve the economic viability, the process operation is pushed to the highest possible column loading that still achieves separation [5]. The associated elution profiles of an overloaded preparative chromatographic operation have an enhanced tendency to overlap, caused by nonlinear displacement or tag-along phenomena [6], and the determination of two essential fractionation interval endpoints with reproducible selectivity is critical [7]. In this context, the main objective of this study is to develop a novel model-based methodology for open-loop optimal control of batch HPLC separation processes. The generic optimal control strategy allows for optimization of

* Corresponding author.
E-mail addresses: anders.holmqvist@chemeng.lth.se (A. Holmqvist), fredrik.magnusson@control.lth.se (F. Magnusson).

http://dx.doi.org/10.1016/j.jprocont.2016.08.002
0959-1524/

process productivity and selectivity with respect to optimal solvent composition trajectories and fractionation interval endpoints while fulfilling the constraint imposed on purity of the target component fractionation.

1.1. Solvent composition trajectory elution strategies

Solvent composition trajectory elution is widely applied in both analytical and preparative chromatography, and refers to a continuous change in the mobile phase during separation [8]. By this means, improved resolution of highly complex sample mixtures can be obtained in a much shorter time than could be expected in isocratic elution conditions. Additionally, peak widths and overloaded band profiles are thinner, allowing better resolution and sample purification [9]. The modulation of the solvent strength during trajectory elution operation can be divided into three generic elution modes. Most frequently the solvent strength at the column inlet is altered proportional to time [10,11]. Alternatively, various types of step trajectories [12] or more sophisticated concave or convex trajectories [13] are applied. In any case, column regeneration and re-equilibration, which can be further divided into the state of *repeatable* [14] and *full equilibration* [15], is mandatory prior to the subsequent injection [16,17].

Most studies on trajectory operation are devoted to quantify and optimize linear trajectories with respect to various performance indices that facilitate quantitative evaluation of the quality and the cost of separation (e.g. production rates, recovery yields and target component purity), see, for example, [18,19] and the references cited therein. Moreover, the results obtained in [20,21] emphasize that concave/convex trajectory elution possesses the potential to outperform conventional isocratic operation and linear trajectories in preparative chromatography.

1.2. PDE-constrained dynamic optimization

In this study, the realistic multi-component system dynamics required for analysis were generated by numerical solution of the *reaction–dispersive model* [22]. This model is governed by a set of mass-balance partial differential equations (PDEs), with a modified Langmuir isotherm and experimentally validated kinetics. The proposed model-based methodology for robust optimal control implies formulating and solving a large-scale dynamic optimization problem (DOP) constrained by PDEs [23,24]. Optimal design, optimal control, and parameter estimation of systems governed by PDE give rise to a class of problems known as PDE-constrained optimization [25]. The size and complexity of the discretized PDEs often pose significant challenges for contemporary optimization methods. There exists two generic *direct methods* to transcribe the infinite DOP into a finite dimensional nonlinear program (NLP); *sequential* and *simultaneous* [26,27]. Optimization studies of batch HPLC separations carried out in the literature have exclusively been using sequential methods, where the system dynamics constraint is handled by embedded numerical integrators, and where the PDEs are approximated using the method-of-lines [28,29] and Galerkin finite element or finite volume methods. Both gradient-based NLP solvers (e.g. sequential quadratic programming and interior-point methods) [30–32] and those based on derivative-free heuristic approaches (e.g. genetic algorithm and simulated annealing) [33,34] have been used successfully.

1.3. Dynamic optimization problem transcription using direct collocation

This contribution describes the realization of a novel open-loop optimal control framework for batch chromatographic separation processes. It is based on a developed simultaneous method where both the control and state variables are fully discretized in the temporal domain using direct local collocation on finite elements [26]. In order to reduce the size of the resulting NLP, the PDE system was approximated using an adaptive, high-order finite volume weighted essentially non-oscillatory (WENO) scheme [35–37]. The WENO scheme is especially suitable for approximating the PDE system considered here, containing both strong discontinuities and complex smooth solution features. The NLP is subsequently solved using the primal-dual interior point method IPOPT [38] and algorithmic differentiation (AD) techniques [39].

Jacobians are required by gradient-based NLP algorithms and simulation. Access to accurate Jacobians often improves the performance and robustness of algorithms, and in addition, efficient implementation of Jacobian computations can reduce the over-all execution time. In the context of HPLC system modeling, Püttmann et al. [40] compared the accuracy of Jacobians, with respect to an intrinsic model parameter, computed using first-order finite differences (FD) and AD. It was shown in that study the AD approach outperformed the FD approach in terms of both accuracy and overall execution time when computing forward sensitivities of the differential algebraic equation (DAE) system, i.e. the linearization of the original system with respect to an intrinsic model parameter. The AD approach in [40] is extended in this study to include computations of Hessians required by the NLP solver.

Simultaneous methods based on direct collocation have been applied for computing cyclic-steady-state (CSS) operation of the continuous *simulated moving bed* (SMB) process [32,41–45]. However, within the scope of batch chromatographic separation processes, the full discretization approach has previously only been used in parameter estimation studies [46]. There is one main reason for considering a simultaneous method in this application. The periodicity criteria arising from cyclic batch operation are straightforward to incorporate in the DOP formulation using a simultaneous method. Alternatively, the CSS solution may also be computed using a sequential method, where the DAE system is integrated repeatedly until the discrepancies of the state variables (spatial column profiles) at initial and final time fulfill a specified tolerance. However, it was shown in [32] that the simultaneous method was superior to the sequential method for solving optimization problems of SMB processes. This conclusion was attributed to the fact that the number of sensitivity equations is large due to the large number of state variables, making the computational effort of integration expensive.

For the purpose of this study, discretizing the entire temporal domain of a complete cyclic operation not only provides the ability to optimize the eluent trajectory but also enables the control over the subsequent regeneration and re-equilibration modes. This is important since a major disadvantage of trajectory elution in terms of production rate results from the need to adequately regenerate and re-equilibrate the column to ensure CSS repeatability in retention time [16]. Hence, minimizing the time for regeneration and re-equilibration in trajectory elution is critical in order to reduce the overall cycle time and, thereby, to enhance the overall production rate [20].

1.4. Aim and scope

The main contribution of this paper is the open-loop optimal strategy and the tools and methods developed for solving the large-scale DOP of batch chromatographic separation processes with respect to a zero-order hold control and fractionation interval endpoints. The parameterized control trajectory enables the introduction of an arbitrary number of degrees of freedom in the DOP. This paper thereby demonstrates the applicability and gain in extending the concepts beyond the conventional elution trajectories previously outlined in Section 1.1. In this regard, the advantages

of this optimal control framework are highlighted through the solution of a challenging ternary mixture separation problem, with human insulin analogs (insulin aspart, desB30 insulin and insulin methyl ester) and the intermediately eluting component as the target, for a hydrophobic interaction chromatography (HIC) [47,48] system. In order to assess the performance of the general elution trajectories, these were benchmarked with conventional linear trajectories. The study presented here had three main objectives:

(i) To develop a novel open-loop optimal control strategy for computing general elution trajectories in order to resolve complex sample mixtures and enhance recovery yield and production rate of batch HPLC separation systems.
(ii) To formulate a DOP, in which the parameterized elution trajectory and target component fractionation interval endpoints are simultaneously optimized, and the periodicity criteria arising from cyclic batch operation is fulfilled.
(iii) To develop numerically efficient tools and methods for transcribing the PDE-constrained DOP into an NLP by combining high-order spatial discretization schemes with direct local collocation in time, and to demonstrate a solution strategy with a state-of-the-art NLP solver and algorithmic differentiation.

1.5. Outline of the paper

The remainder of this paper is structured as follows: Section 2 presents the HPLC separation system. Section 3 outlines the HPLC separation process model and the fundamentals of the spatial discretization scheme. Section 4 describes the open-loop optimal control strategy and formulates the specifications of the DOP. Section 5 outlines the transcription of the DOP into an NLP using direct local collocation, while Section 6 describes the modeling and optimization environment. Section 7 presents the primary results, and Section 8 contains concluding remarks and perspectives for future research.

2. Process description

The HPLC separation system operated in batch mode is characterized by subsequent pulse injections of the sample mixture and relies on pumps to pass a pressurized liquid solvent containing the sample mixture through a column packed with a solid adsorbent material [49]. A simplified P&ID of the standard HPLC system under consideration is illustrated in Fig. 1. By design, modern HPLC systems enable implementing accurate elution trajectories, u, using several consecutive linear segments with different slopes or a larger number of steps with adjusted step sizes and heights [20]. Hence, by controlling the volume fraction of buffers with different solvent strengths (buffer A to E) the mobile phase modifier concentration, $c_{\mathrm{mix},S}$, is obtained in the mixing unit. The feed, with concentration $c_{\mathrm{load},\alpha}$ and $\alpha \in \{A, B, C\}$, is injected as a rectangular pulse with duration Δt_{load} via a multiport valve. The mobile phase subsequently passes the connecting pipes and a flow distributor before entering the separation column with the system volumetric flow rate $\dot{Q}$. The eluting concentration trajectory is analyzed with a UV detector at the outlet of the column [50], and a fractionating valve is controlled based on the data acquired by the detector to separate the mixture into its components [31]. A detailed description of the HPLC system can be found in [22].

2.1. Inputs and outputs

In this study, open-loop optimal control of a commercial HPLC system (see Fig. 1) is considered. The open-loop trajectories of the manipulated variables are calculated by offline dynamic optimization and the control concept for the HPLC system may be divided into two main blocks.

(i) The HIC column is packed with methacrylate-based resin with phenyl ligands and elution is performed with trajectory of potassium chloride (S = KCl) parametrized with piecewise constant controls. It is noteworthy that the manipulated variable, u, has a corresponding actuator system, i.e. the control signal is in fact a set-point to the actuator system which includes a low-level controller ensuring good set-point tracking. The set-point, u, is a piecewise constant signal updated with frequency φ, giving a total of $N_u = \varphi \cdot (t_f - t_0)$ degrees of freedom for the elution trajectory, where t_0 and t_f are the beginning and end of the temporal domain. The limits for the low-level control signals is approximated by absolute and rate limits on u. It is however notable that the control of the elution trajectory, u, denotes the reference mobile phase modifier concentration in the remainder of this paper.
(ii) The control of the fractionating valve switching times, i.e. the temporal horizon $[\tau_0, \tau_0 + \Delta\tau]$, govern the amount of the collected target component. Hence, the maximum recovery yield, while still fulfilling the constraint imposed on purity of the target component fraction, is to a high extent determined by the manipulating variables of the fractionating interval. A review of strategies for controlling the fractionating interval endpoints and their compatibility with large-scale optimization is thoroughly outlined in [7].

Chromatographic separations cannot easily be controlled by conventional control strategies due to their complex dynamics with long time delays, spatially distributed properties, and switchings [31]. This contribution describes, therefore, the realization of a novel open-loop optimal control framework for batch chromatographic processes. The optimal trajectories can conceivably be used as feed-forward and set-point terms in a local feedback control system or combined with nonlinear model predictive control and online state estimation based on dynamic optimization in the form of moving horizon estimation [51] to cope with deviations due to model uncertainty and disturbances.

3. Mathematical modeling

The mathematical modeling of single chromatographic columns operated in batch elution mode has been extensively described in the literature by several authors (see e.g. [6,22,52,53]). From a mathematical point of view, chromatographic processes may be distinguished on the basis of the adsorption isotherm degree of nonlinearity. Specifically, the computational complexity for solving models with linear isotherms, governed by systems of decoupled differential equations, is considerably lower than those with coupled nonlinear adsorption dependency, such as competitive Langmuir and Bi-Langmuir isotherms [31]. Moreover, the physiochemical phenomena at different length scales splits the model problem neatly into: (i) the macroscopic scale mobile phase dynamics governing the concentration trajectories in the flow direction, (ii) the microscopic scale interparticle pore diffusion towards the liquid–solid interface, and (iii) the atomic scale stationary phase dynamics governing the adsorption equilibrium at the liquid–solid interface. The coupling between the spatial scales is bidirectional and several standard models are available for describing mass transport phenomena and multi-component competitive adsorption at the different scales, see e.g. [6] for a thorough review and classification of different modeling approaches.

The most difficult part in the mathematical modeling formulation of chromatographic separations is the determination of

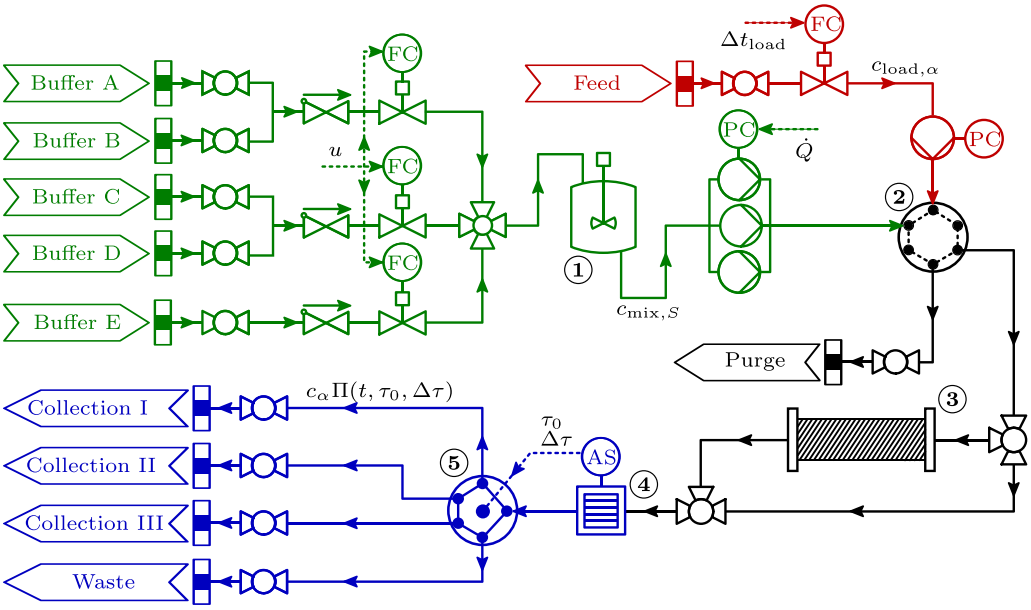

Fig. 1. Simplified P&ID of the HPLC system. Elementary system component description: (1) buffer mixing unit, (2) high-pressure switching valve unit, (3) HPLC separation column, (4) UV detector, and (5) fractionating valve.

the model parameters [54]. In this study, the set of parameters associated with the adsorption's dependency on mobile phase concentrations and the properties of the solvent and the stationary phase was calibrated to lab-scale experimental data by means of the inverse method [53,55–57]. A detailed description of the experimental design and the materials used is outlined in [58], and the least-square estimates of the adsorption isotherm kinetics along with the HPLC system component specifications are listed in Tables 1 and 2, respectively.

3.1. Mobile phase mass transport model

Under the assumptions of infinitely fast diffusion into the particles and rate-limiting adsorption kinetics, the transport of components through the column is described by the *reaction–dispersive model* [6,60]. Thus, the governing equations of the mobile phase defined in the spatial, $z \in [z_0, z_f]$, and temporal, $t \in [t_0, t_f]$, domains are:

$$\frac{\partial c_\alpha}{\partial t} + \frac{(1-\varepsilon_c)}{\varepsilon_t}\frac{\partial q_\alpha}{\partial t} = -\frac{\partial}{\partial z}\left(c_\alpha v_{\text{int}} - \mathcal{D}_{\text{app}}\frac{\partial c_\alpha}{\partial z}\right), \tag{1}$$

where c_α and q_α are the mobile and stationary phase concentration of component $\alpha \in \{A, B, C, S\}$, v_{int} denotes the interstitial velocity of the fluid, $\mathcal{D}_{\text{app}}$ the apparent dispersion coefficient, and ε_c and ε_t the column and apparent total void fractions. Moreover, the apparent dispersion coefficient is derived from flow-rate-dependent correlation and the particle Peclet number, Pe, for column dispersion [59]. Eq. (1) is complemented with Danckwerts boundary conditions, which are written:

$$c_\alpha(t, z_0)v_{\text{int}} - \mathcal{D}_{\text{app}}\frac{\partial c_\alpha}{\partial z}(t, z_0) = \begin{cases} c_{\text{load},\alpha} v_{\text{int}} \Pi(t, t_0, \Delta t_{\text{load}}) & \text{if } \alpha \in \{A, B, C\}, \\ c_{\text{mix},S} v_{\text{int}} & \text{if } \alpha = S, \end{cases} \tag{2}$$

$$\frac{\partial c_\alpha}{\partial z}(t, z_f) = 0. \tag{3}$$

Eq. (2) states that the total mass flux of each component $\alpha \in \{A, B, C\}$ at the column inlet, $z = z_0$, is governed by the injected feed concentration, $c_{\text{load},\alpha}$, and the rectangular function, $\Pi(t, t_0, \Delta t_{\text{load}}) \in \{0, 1\}$, in the temporal horizon $[t_0, \Delta t_{\text{load}}]$. Hence, the loaded sample amount of component α, from temporal integration of the right hand side in Eq. (2), is $\delta_{\text{load},\alpha} = A_c v_{\text{int}} c_{\text{load},\alpha} \Delta t_{\text{load}}$. Moreover, the

Table 1
Nominal HPLC system component design parameters and HIC column specifics. The adsorption capacity and the self-association parameters listed are equal for all insulin variants $\alpha \in \{A, B, C\}$.

Parameter	Description	Value	Unit
$\dot{Q}$	Volumetric flow rate	$6.0 \cdot 10^{-5}$	$\text{m}^3\,\text{s}^{-1}$
Δt_{load}	Sample load duration	$1.0 \cdot 10^{-2}$	s
V_{mix}	Buffer mixing unit volume	$2.0 \cdot 10^{-7}$	m^3
L_c	Column length	$1.0 \cdot 10^{-1}$	m
D_c	Column diameter	$1.0 \cdot 10^{-2}$	m
D_p	Particle diameter	$3.5 \cdot 10^{-5}$	m
ε_c	Interstitial porosity of the column	$3.26 \cdot 10^{-1}$	–
ε_p	Apparent particle porosity	$7.54 \cdot 10^{-1}$	–
ε_t	Total porosity of the column	$\varepsilon_c + (1-\varepsilon_c)\varepsilon_p$	–
$\mathcal{D}_{\text{app}}$ [a]	Apparent dispersion coefficient	$(v_{\text{int}} D_p)\text{Pe}^{-1}$	$\text{m}^2\,\text{s}^{-1}$
v_{int}	Interstitial velocity	$4\dot{Q}(D_c^2 \pi \varepsilon_t)^{-1}$	$\text{m}\,\text{s}^{-1}$
k_{kin}	Kinetic rate constant	$3.0 \cdot 10^{-1}$	s^{-1}
K_{eq}	Self-association equilibrium constant	7.56	$(\text{mol}\,\text{m}^{-3})^{-1}$
ν	Stoichiometric constant	$4.82 \cdot 10^{1}$	–
q_{max}	Adsorption capacity	$1.75 \cdot 10^{1}$	$\text{mol}\,\text{m}^{-3}$

[a] Pe is assumed to be constant and equal to 0.50, i.e. molecular diffusion is neglected [59].

Table 2
Kinetic parameters of the Langmuir self-association adsorption model Eq. (5). The feed composition, $c_{\text{load},\alpha}$, is given in fractional weights for each insulin component and the total feed concentration is 2.0×10^1 ($\text{mol}\,\text{m}^{-3}$).

Component	α	$H_{0,\alpha}$ (−−)	γ_α ($\text{m}^3\,\text{mol}^{-1}$)	$c_{\text{load},\alpha}$ (wt%)
Insulin aspart	A	1.14	2.30×10^{-3}	14.9
desB30 insulin	B	1.51	2.39×10^{-3}	59.1
Insulin methyl ester	C	1.78	2.63×10^{-3}	26.0

total mass flux of the modifier, $\alpha = S$, is governed by the dynamics of the mixing unit (see Fig. 1):

$$\tau_{\text{mix}} \frac{\mathrm{d}c_{\text{mix},S}}{\mathrm{d}t} = \left(u(t) - c_{\text{mix},S}\right), \tag{4}$$

where $c_{\text{mix},S}$ is the concentration at the column inlet and $\tau_{\text{mix}} = V_{\text{mix}}\dot{Q}^{-1}$ the residence time. Hence, the homogenization of the elution trajectory, u, is governed by the response of a first-order system. Finally, a homogeneous Neumann boundary condition in Eq. (3) is prescribed at the outlet, $z = z_f$.

3.2. Stationary phase adsorption model

A recent study [58] showed that the insulin variants (listed in Table 2) displayed a strong tendency toward self-association on HIC adsorbents. Hence, the self-association isotherm [61,62] was used describe the hydrophobic interaction and the dynamics of the stationary phase concentration in Eq. (1). This isotherm is based on the Langmuir adsorption equation [63], the amount of component $\alpha \in \{A, B, C\}$ that is adsorbed, q_α, is a function of its concentration in the mobile phase, the modifier concentration, and the number of stationary phase adsorption sites available. As in the steric mass-action model, adsorption of a protein to the surface is balanced by displacement of counter ions [64,65], but proteins can also adsorb by self-association to other proteins of the same species already adsorbed on the surface. Hence, the isotherm is written in kinetic form as:

$$\frac{\partial q_\alpha}{\partial t} = k_{\text{kin}} \left(H_{0,\alpha} \mathrm{e}^{\gamma_\alpha c_S} c_\alpha \left[1 + 2K_{\text{eq}} \mathrm{e}^{\gamma_\alpha c_S} c_\alpha\right] \left[1 - \sum_{\beta \in \{A,B,C\}} \frac{q_\beta}{q_{\max}}\right]^{\nu} - q_\alpha \right), \tag{5}$$

where k_{kin} is the kinetic rate constant, $H_{0,\alpha}$ the Henry's constant, γ_α the solvophobicity parameter, ν the binding charge ratio between the component and the eluting modifier, $q_{\max}$ the maximum concentration of adsorbed components, and K_{eq} the equilibrium constant for self-association.

3.3. Spatial discretization

The equations of the spatially distributed HPLC column model that describe the mobile and stationary phase state dynamics (see Sections 3.1 and 3.2), constitute a system of non-linear PDEs. In this study, the PDE system was approximated using the method-of-lines [28,29] and high-order finite volume WENO scheme [35–37]. The main advantage of this scheme is its capability to achieve high-order accuracy in smooth regions while maintaining stable, nonoscillatory, and sharp discontinuity transitions. In contrast to other high-order spatial discretization schemes that make use of *flux limiters* [66], such as the MUSCL scheme [67] and the TVD scheme [68], the WENO scheme does not require tuning of parameters and more importantly the discretization scheme is twice continuously differentiable; a necessity when employing Newton-based methods for solving NLPs. Although a high-order WENO scheme may use several times more CPU time than the aforementioned schemes, which are usually second-order accurate in the smooth part of the solution [69], it is still computationally advantageous for the purpose of this study where the DOP is transcribed into an NLP using direct collocation in time (see Section 5.2). Hence, less finite volume elements are required to spatially resolve complicated smooth structures with small numerical dissipation, and thereby significantly reducing the size of the resulting NLP.

3.3.1. WENO interpolation and reconstruction

The essential idea of WENO schemes is an adaptive and non-linear interpolation and reconstruction procedure that is used to automatically choose the locally smoothest stencil and thereby avoids crossing discontinuities in the interpolation procedure as much as possible. The spatial horizon is divided into an uniform mesh $z_i = i\Delta z$ with $i \in [1..n_v]$ elements. Let $z_{i+\frac{1}{2}} = \frac{1}{2}(z_i + z_{i+1})$ the half points. For conventional finite volume schemes the numerical solutions are cell averages of the function $\boldsymbol{x}(z)$:

$$\bar{\boldsymbol{x}}_i := \frac{1}{\Delta z} \int_{z_{i-\frac{1}{2}}}^{z_{i+\frac{1}{2}}} \boldsymbol{x}(z)\mathrm{d}z, \tag{6}$$

over the intervals $I_i = (z_{i-\frac{1}{2}}, z_{i+\frac{1}{2}})$. Starting from the location of I_i and the order of accuracy k, a stencil based on $(2k-1)$ points yields that there are k candidate sub-stencils given by $S_i := \left\{z_{i-r}, \ldots, z_{i-r+k-1}\right\}$ with $r = [0..k-1]$. Given the k candidate sub-stencils, the following Lagrange interpolation polynomial on each sub-stencil can be defined [70]:

$$\boldsymbol{x}_L^{(r)}(z) = \sum_{j=0}^{k-1} \bar{\boldsymbol{x}}_{i-r+j} \ell_{rj}(z), \tag{7}$$

where $\ell_{rj}(z)$ denotes the coefficients dependent upon the location of z, and are given by:

$$\ell_{rj}(z) = \prod_{\substack{l=0 \\ l \neq j}}^{k-1} \frac{z - z_{i-r+l}}{z_{i-r+j} - z_{i-r+l}}. \tag{8}$$

The $(2k-1)$ point WENO interpolation polynomial of order $(2k-1)$ accuracy can then be formulated as a convex combination of the Lagrange interpolation polynomials from each sub-stencil:

$$\boldsymbol{x}_W(z) = \sum_{r=0}^{k-1} \omega_r(z) \boldsymbol{x}_L^{(r)}(z), \tag{9}$$

where $\omega_r(z) \geq 0$ are the nonlinear weights depending on both the location z and the values of $\bar{\boldsymbol{x}}$ being interpolated and satisfies $\sum_{r=0}^{k-1} \omega_r(z) = 1$. The nonlinear weights are defined in [35] as:

$$\omega_r(z) = \varpi_r(z) \left(\sum_{s=0}^{k-1} \varpi_s(z) \right)^{-1}, \tag{10}$$

$$\varpi_r(z) = \frac{\gamma_r}{\left(\epsilon + \beta_r(z)\right)^2}, \tag{11}$$

where ϵ is a small positive number used to avoid the denominator becoming zero, and where the linear weights γ_r satisfy $\sum_{r=0}^{k-1} \gamma_r = 1$. It is noteworthy that the choice of the unnormalized nonlinear weight ϖ_r defined in Eq. (11) is inversely proportional to the square of the smoothness indicator $\beta_r(z)$. Hence, ϖ_r is smaller if $\beta_r(z)$ is larger, i.e. if the function $\boldsymbol{x}(z)$ in the sub-stencil S_i is less smooth [36]. The smoothness indicator is chosen as in [35]:

$$\beta_r(z) = \sum_{l=1}^{k-1} \Delta z^{2l-1} \int_{z^-}^{z^+} \left(\frac{\mathrm{d}^l}{\mathrm{d}z^l} \boldsymbol{x}_L^{(r)}(z) \right)^2 \mathrm{d}z, \tag{12}$$

where the limits of the integration are chosen based upon the location of z in relation to the interpolation points z_j with $j = [i - (k-1). . i + (k-1)]$. The scaling factor Δz^{2l-1} is to make sure that the final explicit formulas for the smoothness indicators is independent of the mesh size, Δz.

To reconstruct the first-order spatial derivatives, $\mathrm{d}\boldsymbol{x}_W(z)/\mathrm{d}z$, (evaluated to form the diffusion term in Eq. (1)), a central stencil is used and the approximation is expressed as a linear combination of the point values in that stencil [71]. Contrarily, the interpolation in Eq. (9) was solely based upon nonlinear weights. However, the

diffusion term in Eq. (1) is dissipative in nature, and for this reason it was proven reasonable in [72] to use linear weights rather than WENO weights in Eq. (9). Finally, the explicit formulas of the Lagrange interpolation polynomials in Eq. (7), smoothness indicators and linear weights can be readily found in [36] for $k \in [1, 7]$.

4. Open-loop optimal control strategy

The cyclic operation of HPLC separation processes in batch elution mode imposes adequate retention time repeatability by conditioning the column to the initial modifier concentration prior to the subsequent injection [16,17]. This implies computing limit cycle dynamic solutions that conform to the CSS periodicity criteria over the processing cycle. In the scope of chromatographic separations, CSS predictions have previously only been applied to continuous SMB [73] and *multicolumn counter-current solvent gradient purification* (MCSGP) [74,75] processes. Therefore, the open-loop optimal control strategy developed in this study for simultaneous optimization of elution trajectories and target component fractionating interval endpoints uses a direct method for the computation of a CSS solution of the *reaction–dispersive model* outlined in Section 3. Hence, the inclusion of CSS periodicity constraints in the DOP ensures that the elution trajectory is bound to converge to the optimal CSS, and equally important, enables control over the column regeneration and re-equilibration modes. Consequently, the comprehensive DOP formulation enables minimization of those time periods, while fulfilling the CSS periodicity criteria and the constraint imposed on purity of the target component fractionation, and thereby reduces the overall cycle time and ultimately enhances the cyclic productivity.

It is however noteworthy that in order for the comprehensive CSS description to be experimentally feasible, a representation of the most retained component in the loaded sample mixture is required. This is vital for prohibiting stationary phase accumulation of otherwise irreversibly adsorbing components (impurities), causing a gradual decrease in column adsorption capacity, and for obtaining long-term cycle-to-cycle retention time reproducibility. The advantages and applicability of this open-loop optimal control framework is therefore highlighted through the solution to two different control strategies:

(i) *Optimal control strategy I* is exclusively concerned with the batch elution operation mode and the periodicity constraints are relaxed.
(ii) *Optimal control strategy II* is concerned with the comprehensive CSS operation mode and the temporal horizon includes the column regeneration and re-equilibration modes.

Hence, *optimal control strategy I* that considerably reduces the DOP complexity is preferable when the complete sample mixture composition is unknown. This strategy is therefore extensively applied in open-loop optimal control studies on non-isocratic batch elution chromatography, see, for example, [21,19] and the references cited therein.

4.1. Cyclic-steady-state criteria formulation

The computation of CSS solutions over the temporal horizon $t \in [t_0, t_f]$ requires that Eqs. (1)–(5) are augmented with additional important criteria governing that the state at the initial time is retained at the end of the cycle. Accordingly, the CSS criteria can be expressed by the periodicity constraints:

$$0 = \int_{t_0}^{t_f} \nu_{\text{int}} A_c c_\alpha(t, z_f)\mathrm{d}t - \delta_{\text{load},\alpha}, \tag{13a}$$

$$0 = c_S(t_0, z) - c_S(t_f, z), \quad \forall z \in [z_0, z_f], \tag{13b}$$

$$0 = c_{\text{mix},S}(t_0) - c_{\text{mix},S}(t_f), \tag{13c}$$

$$0 = u(t_0) - u(t_f), \tag{13d}$$

and initial conditions satisfying:

$$0 = c_S(t_0, z) - u(t_0), \quad \forall z \in [z_0, z_f], \tag{13e}$$

$$0 = c_{\text{mix},S}(t_0) - u(t_0). \tag{13f}$$

Specifically, Eq. (13a) states the flux of the most retained component α at the column outlet, $z = z_f$, needs to be equal to its total loaded sample amount, $\delta_{\text{load},\alpha}$, at final time. This criterion, thereby, ensures that all components are completely eluted at the end of time horizon. The equality constraints (13b)–(13d) govern that the modifier concentration, c_S, at every column position $z \in [z_0, z_f]$ as well as the concentration in the mixing unit, $c_{\text{mix},S}$, are consistent at the initial and terminal times. Moreover, Eqs. (13e) and (13f) are supplementary initial conditions, enforcing the initial modifier concentration at t_0. Eqs. (13a)–(13d) are introduced in the DOP whereas Eqs. (13e) and (13f) are introduced as initial values in the governing mobile phase transport equations. Although the periodicity constraints only consider the dynamics of the mobile phase, it is noteworthy that the state of the stationary phase is inherently comprehended in this formalism.

4.2. Optimal control problem specifications

The design and the operation of chromatographic separations require the choice and the adaptation of a large number of parameters which affect the separation in a highly nonlinear and interacting fashion [76]. The focus of HPLC process optimization is to determine those operating conditions which maximize various performance indices, which facilitate quantitative evaluation of the quality and the cost of separation [19], while satisfying the target component purity requirement and the additional process constraints. Likewise, there are several competing objectives which require a trade-off to ensure satisfactory design (see e.g. [6] for a thorough review).

Generally, the elution trajectories at the column outlet, $c_\alpha(t, z_f)$ and $\alpha \in \{A, B, C\}$, form the basis for evaluating the objective functions that strongly depend on the amount of target component captured, which in turn is critically influenced by the fractionation interval [7]. In this study, the competing objective functions of yield, Y_α, and productivity, P_α, with the intermediately eluting component $\alpha = B$ as target was considered. Hence, the objective functions of component α collected in the fractionation horizon $[\tau_0, \tau_0 + \Delta\tau]$ are defined as:

$$\delta_{\text{load},\alpha} \frac{\mathrm{d}Y_\alpha}{\mathrm{d}t} = c_\alpha(t, z_f)\nu_{\text{int}} A_c \Pi(t, \tau_0, \Delta\tau), \tag{14}$$

$$P_\alpha(t) = \frac{1}{V_c t_f} \delta_{\text{load},\alpha} Y_\alpha(t), \tag{15}$$

where $\Pi(t, \tau_0, \Delta\tau) \in [0, 1]$ is smooth rectangular function in the fractionation horizon. It is noteworthy that P_α, which is defined as the amount of target component collected per cycle time and scaled to the size of the column, is intrinsically governed by Y_α. Consequently, the feasible CSS solution to the DOP, subject to the periodicity constraints defined in Eq. (13), over a fixed temporal horizon $[t_0, t_f]$ represents the solution to a bi-objective optimization problem. In the context of periodic PDE constrained multi-objective

optimal control problems, there are several deterministic strategies available which provide fast and efficient generation of the Pareto optimal solution set, see e.g. [77] for interactive methods and [78] for recent scalarization approaches and the references therein. However, for the purpose of this study a weighted sum scalarization method was used to combine the objectives in Eqs. (14) and (15) into a single performance index with a weight $\omega \in [0, 1]$. This allowed the use of deterministic NLP routines and ensured an accurate and efficient Pareto set generation. Moreover, apart from maximizing the bi-objective weighted sum, a quadratic cost on the differences of the piecewise constant control flows, Δu, was added in order to influence the smoothness of u. Hence, the resulting cost was defined as:

$$-(\omega P_\alpha(t_f) + (1-\omega) Y_\alpha(t_f)) + R \sum_{j=1}^{N_u - 1} \Delta u_j^2. \tag{16}$$

Eq. (16) has a typical optimal control Mayer term together with a quadratic penalty on the differences of the piecewise constant controls discretized with N_u segments in the temporal domain $[t_0, t_f]$ and R is a weight. The cost function is optimized while fulfilling the requirement imposed on purity of the target component fractionation:

$$X_\alpha(t) = \delta_{\text{load},\alpha} Y_\alpha(t) \left(\sum_{\beta \in \{A,B,C\}} \delta_{\text{load},\beta} Y_\beta(t) \right)^{-1}, \tag{17}$$

where the numerator of the right hand side represents the captured amount of the target component in $[\tau_0, \tau_0 + \Delta\tau]$ and the denominator represents the total amount captured. Hence, the requirement imposed on purity is incorporated in the DOP as a terminal inequality constraint, $X_{\alpha,L} - X_\alpha(t_f) \leq 0$, on the algebraic variable X_α with an assigned lower purity requirement $X_{\alpha,L}$.

4.3. Optimal control problem formulation

Given the optimization specifications in Eq. (14)–(17), the optimal control problem, with differential-algebraic constraints [79,26], over the temporal domain $[t_0, t_f]$ may now be formulated as:

$$\text{min.} \quad -(\omega P_B(t_f) + (1-\omega) Y_B(t_f)) + R \sum_{j=1}^{N_u - 1} \Delta u_j^2, \tag{18a}$$

$$\begin{aligned}
\text{w.r.t.} \quad & \boldsymbol{x} : [t_0, t_f] \to \mathbb{R}^{n_x}, && \boldsymbol{y} : [t_0, t_f] \to \mathbb{R}^{n_y}, \\
& \boldsymbol{p} \in \mathbb{R}^{n_p}, && u_m \in \mathbb{R}, \\
\text{s.t.} \quad & \boldsymbol{F}(t, \dot{\boldsymbol{x}}(t), \boldsymbol{x}(t), \boldsymbol{y}(t), u(t), \boldsymbol{p}) = \boldsymbol{0}, && \boldsymbol{x}(t_0) = \boldsymbol{x}_0, && (18b) \\
& \boldsymbol{g}_e(\boldsymbol{x}(t_0), \boldsymbol{x}(t_f), u_1, u_{N_u}) = \boldsymbol{0}, && && (18c) \\
& X_{B,L} - X_B(t_f) \leq 0, && \boldsymbol{p}_L \leq \boldsymbol{p} \leq \boldsymbol{p}_L, && (18d) \\
& u_L \leq u_m \leq u_U, && |\Delta u_n| \leq \Delta u_U, \\
& \forall m \in [1..N_u], && \forall n \in [1..N_u - 1], \quad \forall t \in [t_0, t_f], && (18e)
\end{aligned}$$

where $u(t)$ is the discrete setpoint u_m at time t and $\Delta u_n := u_{n+1} - u_n$. In addition to the discrete controls u_m and the free manipulated parameters $\boldsymbol{p} = (\tau_0, \Delta\tau)$, the optimization variables include the state variables $\boldsymbol{x}(t) = (c_\alpha(t, z_j), c_S(t, z_j), c_{\text{mix},S}(t), q_\alpha(t, z_j), Y_\alpha(t))$ for $\alpha \in \{A, B, C\}$ as well as the algebraic variables $\boldsymbol{y}(t) = (X_B(t), P_B(t))$. $\boldsymbol{F}$ denotes the implicit DAE system resulting from the spatially discretized PDE system with the WENO scheme on a uniform mesh (see Section 3.3). Moreover, $\boldsymbol{g}_e$ denotes the point equality constraints and assembles the CSS periodicity constraints defined in Eq. (13) and absolute and rate limitations of the control are enforced in Eq. (18e).

It is noteworthy that the modifier elution trajectory, u, and the fractionation interval manipulated variables are simultaneously optimized in the optimal control problem (18) subject to the DAE system dynamics and the purity inequality constraint. Contrarily, the fractionation interval manipulated variables are usually treated independently of DAE system dynamics in the published literature. As described in [5,7], a decomposition strategy is adopted to transform the DOP into two levels and solved using a sequential method, where the dynamic system constraint is handled by numerical integrators. Thus, given the dynamic system response, the fractionating interval endpoints decision is performed in a lower-level optimization problem embedded within an upper-level NLP targeting various process objectives with respect to the process operating and design variables. By these means, the target component purity inequality constraint and the fractionating interval optimization variables are eliminated form the upper-level NLP and considerably reduces its complexity. However, it is not expedient to consider the aforementioned decomposition strategy for the purpose of this study, where the shape of the optimal elution trajectories are highly intercorrelated with the fractionation interval endpoints.

4.3.1. Bilevel optimal control problem decomposition

The optimization variables of the optimal control problem (18) reflect the set of manipulating variables needed to be online controlled during operation. In this context, this study focuses on the accurate computation of general elution trajectories and fractionation interval endpoints of an intermediately eluting component from a multi-component mixture. Hence, the comprehensive optimal control problem with respect to all process operating parameters is beyond the scope of this study. However, the optimal open-loop controlled trajectories are to a high degree governed by the additional process operation parameters (see Fig. 1 and Table 1), which in turn are governed by the competing objective functions in Eqs. (14) and (15). It is nonetheless straightforward to extend the optimal control problem with additional time-invariant manipulating variables, including $\dot{Q}$ and $c_{\text{load},\alpha}$ for $\alpha \in \{A, B, C\}$. Contrarily, incorporating time-related optimization variables, including t_f and Δt_{load}, significantly increases the computational complexity. This results from the simultaneous solution strategy in which the optimal control problem is transcribed into an NLP using direct local collocation. Specifically, introducing t_f as a free optimization variable yields the formulation of a *minimal time control problem*. The resulting formulation may not be computationally tractable due to the large-scale and nonlinear DAE-constrained dynamics. For these reasons, the comprehensive optimal control problem is cast in the framework of bilevel optimal control where the upper level concerns optimization of Eq. (16) with respect to the set of time-related manipulating variables, $\boldsymbol{q}$, and the optimal control problem (18) augmented with the DAE system dynamics is considered in the lower level:

$$\text{min.} \quad -(\omega P_B(t_f) + (1-\omega) Y_B(t_f)) + R \sum_{j=1}^{N_u - 1} \Delta u_j^2, \tag{19a}$$

$$\text{w.r.t.} \quad \boldsymbol{q} \in \mathbb{R}^{n_q}, \tag{19b}$$

$$\text{s.t.} \quad \boldsymbol{q}_L \leq \boldsymbol{q} \leq \boldsymbol{q}_U,$$

$$(\boldsymbol{x}, u, \boldsymbol{p}) = \text{argmin.} \; -(\omega P_B(t_f) + (1-\omega) Y_B(t_f)) + R \sum_{i=j}^{N_u - 1} \Delta u_j^2, \tag{19c}$$

$$\begin{aligned}
\text{w.r.t.} \quad & \boldsymbol{x} : [t_0, t_f] \to \mathbb{R}^{n_x}, && \boldsymbol{y} : [t_0, t_f] \to \mathbb{R}^{n_y}, \\
& \boldsymbol{p} \in \mathbb{R}^{n_p}, && u_m \in \mathbb{R}, \\
\text{s.t.} \quad & \boldsymbol{F}(t, \dot{\boldsymbol{x}}(t), \boldsymbol{x}(t), \boldsymbol{y}(t), u(t), \boldsymbol{p}, \boldsymbol{q}) = \boldsymbol{0}, && \boldsymbol{x}(t_0) = \boldsymbol{x}_0, && (19d) \\
& \boldsymbol{g}_e(\boldsymbol{x}(t_0), \boldsymbol{x}(t_f), u_1, u_{N_u}) = \boldsymbol{0}, && && (19e)
\end{aligned}$$

$$X_{B,L} - X_B(t_f) \le 0, \qquad \boldsymbol{p}_L \le \boldsymbol{p} \le \boldsymbol{p}_L, \tag{19f}$$

$$u_L \le u_m \le u_U, \quad |\Delta u_n| \le \Delta u_U, \quad \forall m \in [1..N_u],\ \forall n \in [1..N_u - 1], \quad \forall t \in [t_0, t_f]. \tag{19g}$$

By these means, the optimal control problem (18) is solved in the lower-level (19c)–(19g)) for a fixed temporal horizon $[t_0, t_f]$ which considerably reduces the NLP complexity and facilitates scaling of the NLP variables.

5. Numerical solution of dynamic optimization problem

The optimal control problem Eq. (18) falls within the class of dynamic optimization problems of the general form:

$$\min. \quad \int_{t_0}^{t_f} L(t, \boldsymbol{z}(t), \boldsymbol{u}(t), \boldsymbol{p})\,\mathrm{d}t + \phi(\boldsymbol{z}(t_f), \boldsymbol{p}) + \sum_{j=1}^{N_u - 1} (\Delta \boldsymbol{u}_n)^T \boldsymbol{R} (\Delta \boldsymbol{u}_n), \tag{20a}$$

$$\text{w.r.t.} \quad \boldsymbol{x} : [t_0, t_f] \to \mathbb{R}^{n_x}, \quad \boldsymbol{y} : [t_0, t_f] \to \mathbb{R}^{n_y}, \quad \boldsymbol{p} \in \mathbb{R}^{n_p}, \quad \boldsymbol{u}_m \in \mathbb{R}^{n_u},$$

$$\text{s.t.} \quad \boldsymbol{F}(t, \boldsymbol{z}(t), \boldsymbol{u}(t), \boldsymbol{p}) = \boldsymbol{0}, \quad \boldsymbol{x}(t_0) = \boldsymbol{x}_0, \tag{20b}$$

$$\boldsymbol{z}_L \le \boldsymbol{z}(t) \le \boldsymbol{z}_U, \quad \boldsymbol{p}_L \le \boldsymbol{p} \le \boldsymbol{p}_U, \tag{20c}$$

$$\boldsymbol{u}_L \le \boldsymbol{u}_m \le \boldsymbol{u}_U, \quad \Delta \boldsymbol{u}_L \le \Delta \boldsymbol{u}_n \le \Delta \boldsymbol{u}_U, \tag{20d}$$

$$\boldsymbol{g}_e(\boldsymbol{x}(t_0), \boldsymbol{x}(t_f), \boldsymbol{u}_1, \boldsymbol{u}_{N_u}, \boldsymbol{p}) = \boldsymbol{0}, \quad \boldsymbol{g}_i(\boldsymbol{x}(t_0), \boldsymbol{x}(t_f), \boldsymbol{u}_1, \boldsymbol{u}_{N_u}, \boldsymbol{p}) \le \boldsymbol{0}, \quad \forall t \in [t_0, t_f], \quad \forall m \in [1..N_u], \forall n \in [1..N_u - 1] \tag{20e}$$

where $\boldsymbol{x}$ is the differential variable, $\boldsymbol{y}$ is the algebraic variable, $\boldsymbol{u}$ is the control variable, $\boldsymbol{p}$ is the free time-invariant parameters, and $\boldsymbol{z} := (\dot{\boldsymbol{x}}, \boldsymbol{x}, \boldsymbol{y})$ is the composition of the internal system variables. The objective Eq. (20a) is a typical optimal control Bolza functional together with a quadratic penalty on $\Delta \boldsymbol{u}_n$, where $\boldsymbol{R} \in \mathbb{R}^{n_u \times n_u}$ acts as a weight and is typically diagonal. The optimization variables are the free operating parameters – the discrete control signal $\boldsymbol{u}$ and free time-invariant parameters $\boldsymbol{p}$ – and the trajectories $\boldsymbol{x}$ and $\boldsymbol{y}$. The trajectories are determined by the free operating parameters via the implicit DAE system in Eq. (20b). Assuming that the DAE system is of index one, which holds for Eq. (18b), consistent initial conditions are obtained by specifying the initial value of the differential variable. Consequently, $\boldsymbol{x}$ corresponds to the state of the system, and will henceforth be referred to as such. Time-invariant bounds on variables are introduced in Eq. (20c). Bounds on $\boldsymbol{u}_m$ and $\Delta \boldsymbol{u}_n$ are introduced in Eq. (20d). Finally, terminal and initial constraints on equality and inequality form are introduced in Eq. (20e).

The remainder of this section outlines common numerical methods for solving Eq. (20) and thoroughly presents the method that was employed to solve Eq. (18), which is based on direct local collocation.

5.1. Numerical methods for dynamic optimization

There are many approaches to solving dynamic optimization problems in the form of Eq. (20), which stem from the theory of optimal control. The most widely used techniques today are based on first-order necessary conditions for local optimality, of which a survey is available in e.g. [80]. The first dichotomy of these methods is that of *indirect* and *direct* methods. Indirect methods start by establishing the optimality conditions, and then discretize the problem to find a numerical solution. These methods are often difficult to employ due to needing good initial guesses of costates and also manual identification of the switching structure of inequalities. Direct methods instead first discretize the dynamics, thus reducing the dynamic optimization problem to an NLP of the general form:

$$\begin{aligned} &\min. && f(\boldsymbol{x}), && \text{(21a)}\\ &\text{w.r.t.} && \boldsymbol{x} \in \mathbb{R}^{n_x}, \\ &\text{s.t.} && \boldsymbol{x}_L \le \boldsymbol{x} \le \boldsymbol{x}_U, && \text{(21b)}\\ & && \boldsymbol{g}(\boldsymbol{x}) = \boldsymbol{0}, && \text{(21c)}\\ & && \boldsymbol{h}(\boldsymbol{x}) \le \boldsymbol{0}. && \text{(21d)} \end{aligned}$$

The optimality conditions are then given by the Karush–Kuhn–Tucker (KKT) conditions.

The second dichotomy is that of *sequential* and *simultaneous* discretization techniques. The three most common techniques for direct methods are single shooting, multiple shooting, and collocation [26,27]. Direct single shooting is a purely sequential method which parametrizes the control, using e.g. polynomials or piecewise constant functions, and then uses the control parameters as optimization variables. The system dynamics constraint corresponding to Eq. (20b) is handled by embedded numerical integrators, which also provide sensitivities that are used to iteratively update the control parameters. The numerical robustness of single shooting can be improved by dividing the time horizon into subintervals, and then essentially employing single shooting within each such interval, which leads to the method of multiple shooting.

Finally there are simultaneous methods. These methods encode the discretized equations and variables as NLP constraints and variables. Consequently, they do not rely on embedded numerical integrators. In this paper we focus on collocation methods. See [27] for details on other simultaneous methods.

5.2. Direct local collocation

In this study, direct local collocation [26,81] was employed to solve Eq. (18). The fundamental idea of the method is to discretize the differential equations using finite differences, thus transforming, or *transcribing*, the infinite-dimensional dynamic optimization problem into a finite-dimensional NLP. The discretization scheme is based on collocation methods, which are special cases of implicit Runge–Kutta methods and are also commonly used for numerical solution of DAE and stiff ordinary differential equation (ODE) systems [82].

5.2.1. Collocation polynomials

The optimization time horizon is divided into n_e elements. Let h_i denote the length of element i. The time is normalized in element i according to:

$$\tilde{t}_i(\tau) := t_{i-1} + h_i \cdot (t_f - t_0) \cdot \tau, \quad \tau \in [0, 1], \quad \forall i \in [1..n_e], \tag{22}$$

where τ is the normalized time, $\tilde{t}_i(\tau)$ is the corresponding unnormalized time, and t_i is the mesh point (right boundary) of element i. This normalization enables a treatment of the below interpolation conditions that is homogeneous across elements. Within element i the time-continuous variable $\boldsymbol{z}$ is approximated using a polynomial in the local time τ denoted by:

$$\boldsymbol{z}_i = (\dot{\boldsymbol{x}}_i, \boldsymbol{x}_i, \boldsymbol{y}_i) : [0, 1] \to \mathbb{R}^{n_z},$$

which is called the collocation polynomial for that element, where $n_z := 2n_x + n_y$. The collocation polynomials are formed by choosing n_c collocation points, which are chosen to be the same for all elements. In this study, Lagrange interpolation polynomials are used to represent the collocation polynomials, which in turn make us of the collocation points as interpolation points. Hence, let $\tau_k \in [0, 1]$ denote collocation point $k \in [1..n_c]$, and let $\boldsymbol{z}_{i,k} = (\dot{\boldsymbol{x}}_{i,k}, \boldsymbol{x}_{i,k}, \boldsymbol{y}_{i,k}) \in \mathbb{R}^{n_z}$ denote the value of $\boldsymbol{z}_i(\tau_k)$.

Optimal control problems usually involve finding an optimal time-continuous control signal, in which case the control signal is also approximated using collocation polynomials. However, since

a time-discrete control signal $\boldsymbol{u}$ is considered in this study, there is no need to further parametrize it, since it already resides in the finite-dimensional space $\mathbb{R}^{N_u \cdot n_u}$. To simplify the treatment of $\boldsymbol{u}$ in the discretization procedure in this study, the element distribution is chosen so that every point in time where the control changes value – that is, every multiple of the control frequency φ – coincides with a mesh point. This allows the control signal $\boldsymbol{u}_m$ to be represented by a single variable that corresponds to the constant value of

$$\boldsymbol{u}(t), \quad \forall t \in [t_0 + (m-1)\varphi, t_0 + m\varphi].$$

Since the states need to be continuous on $[t_0, t_f]$, an additional interpolation point is introduced at the start of each element for the corresponding collocation polynomials, denoted by $\tau_0 := 0$. The collocation polynomials within element i are thus given by:

$$\boldsymbol{x}_i(\tau) = \sum_{k=0}^{n_c} \boldsymbol{x}_{i,k} \cdot \tilde{\ell}_k(\tau), \quad \boldsymbol{y}_i(\tau) = \sum_{k=1}^{n_c} \boldsymbol{y}_{i,k} \cdot \ell_k(\tau), \quad \forall i \in [1..n_e], \quad (23)$$

where $\tilde{\ell}_k$ and ℓ_k are Lagrange basis polynomials, respectively with and without the additional interpolation point τ_0. The collocation polynomials are thus parametrized by the values $\boldsymbol{z}_{i,k} = \boldsymbol{z}_i(\tau_k)$. In order to obtain the collocation polynomial for the state derivative $\dot{\boldsymbol{x}}$ in element i, the collocation polynomial $\boldsymbol{x}_i$ is differentiated with respect to time. Finally, there are different schemes for choosing the collocation points τ_k, with different numerical properties, in particular regarding stability and order of convergence. The most common ones are called Gauss, Radau and Lobatto collocation [82]. The direct method in this study makes use of Radau collocation, which always places a collocation point at the end of each element, and the rest are chosen in a manner that minimizes the quadrature error.

5.2.2. Transcription of the dynamic optimization problem

In this section the dynamic optimization problem Eq. (20) is transcribed into an NLP, using the collocation polynomials constructed above. The optimization domain of functions on $[t_0, t_f]$, which is infinite-dimensional, is thus reduced to a domain of finite dimension by approximating the trajectory $\boldsymbol{z}$ by a piecewise polynomial function. As decision variables in the NLP we choose the system variable values in all the collocation points, $\boldsymbol{z}_{i,k}$, the discrete control signal, $\boldsymbol{u}_m$, the state at the start of each element, $\boldsymbol{x}_{i,0}$, and the free parameters $\boldsymbol{p}$. The transcription of Eq. (20) then results in the NLP:

$$\min. \sum_{i=1}^{n_e} h_i \sum_{k=1}^{n_c} \omega_k L\left(t_{i,k}, \boldsymbol{z}_{i,k}, \boldsymbol{u}_{\Gamma(i)}, \boldsymbol{p}\right) + \phi(\boldsymbol{z}_{n_e,n_c}, \boldsymbol{p}) + \sum_{j=1}^{N_u-1} (\Delta \boldsymbol{u}_j)^T \boldsymbol{R} (\Delta \boldsymbol{u}_j) \quad (24a)$$

$$\begin{aligned}
&\text{w.r.t.} && \boldsymbol{z}_{i,k} \in \mathbb{R}^{n_z}, \quad \boldsymbol{x}_{i,0} \in \mathbb{R}^{n_x}, && \boldsymbol{u}_m \in \mathbb{R}^{n_u}, \quad \boldsymbol{p} \in \mathbb{R}^{n_p}, && (24b)\\
&\text{s.t.} && \boldsymbol{F}(t_{i,k}, \boldsymbol{z}_{i,k}, \boldsymbol{u}_{\Gamma(i)}, \boldsymbol{p}) = \boldsymbol{0}, && \boldsymbol{x}_{1,0} = \boldsymbol{x}_0, && \\
& && \boldsymbol{z}_L \le \boldsymbol{z}_{i,k} \le \boldsymbol{z}_U, && \boldsymbol{p}_L \le \boldsymbol{p} \le \boldsymbol{p}_U, && (24c)\\
& && \boldsymbol{u}_L \le \boldsymbol{u}_m \le \boldsymbol{u}_U, && \Delta \boldsymbol{u}_L \le \Delta \boldsymbol{u}_n \le \Delta \boldsymbol{u}_U, && (24d)\\
& && \boldsymbol{g}_e(\boldsymbol{x}_{1,0}, \boldsymbol{x}_{n_e,n_c}, \boldsymbol{u}_1, \boldsymbol{u}_{N_u}, \boldsymbol{p}) = \boldsymbol{0}, && \boldsymbol{g}_i(\boldsymbol{x}(t_0), \boldsymbol{x}(t_f), \boldsymbol{u}_1, \boldsymbol{u}_{N_u}, \boldsymbol{p}) \le \boldsymbol{0}, && (24e)
\end{aligned}$$

$$\dot{\boldsymbol{x}}_{i,k} = \frac{1}{h_i} \sum_{l=0}^{n_c} \boldsymbol{x}_{i,l} \frac{\mathrm{d}\tilde{\ell}_l}{\mathrm{d}\tau}(\tau_k), \quad (24f)$$

$$\begin{aligned}
&\boldsymbol{x}_{j-1,n_c} = \boldsymbol{x}_{j,0}, && \forall j \in [2..n_e], && (24g)\\
&\forall i \in [1..n_e], \forall k \in [1..n_c], && \forall m \in [1..N_u], \forall n \in [1..N_u - 1]. &&
\end{aligned}$$

The transcription of the Lagrange term in the objective utilizes Gauss–Radau quadrature within each element to approximate the integral by a sum:

$$\begin{aligned}
&\int_{t_0}^{t_f} L(t, \boldsymbol{z}(t), \boldsymbol{u}(t), \boldsymbol{p})\,\mathrm{d}t \\
&= \sum_{i=1}^{n_e} \int_{t_{i-1}}^{t_i} L(t, \boldsymbol{z}(t), \boldsymbol{u}_{\Gamma(i)}, \boldsymbol{p})\,\mathrm{d}t \\
&\approx \sum_{i=1}^{n_e} h_i \sum_{k=1}^{n_c} \omega_k L\left(t_{i,k}, \boldsymbol{z}(t_{i,k}), \boldsymbol{u}_{\Gamma(i)}, \boldsymbol{p}\right) \\
&\doteq \sum_{i=1}^{n_e} h_i \sum_{k=1}^{n_c} \omega_k L\left(t_{i,k}, \boldsymbol{z}_{i,k}, \boldsymbol{u}_{\Gamma(i)}, \boldsymbol{p}\right),
\end{aligned}$$

where $\Gamma(i)$ is the index m corresponding to the control value $\boldsymbol{u}_m$ for element i, $t_{i,k} := \tilde{t}_i(\tau_k)$ denotes the unnormalized collocation point k in element i, ω_k is the quadrature weight, and $a \doteq b$ denotes that b, which belongs to Eq. (24), is the corresponding transcription of a, which belongs to Eq. (20). The two remaining terms in the objective are straightforward to transcribe. The objective Eq. (20a) is thus transcribed into Eq. (24a).

The essence of direct collocation is in the transcription of the system dynamics constraint Eq. (20b). Instead of enforcing the DAE system for all times $t \in [t_0, t_f]$, it is only enforced at the collocation points. Thus

$$\begin{aligned}
&\boldsymbol{F}(t, \boldsymbol{z}(t), \boldsymbol{u}(t), \boldsymbol{p}) = \boldsymbol{0}, && \forall t \in [t_0, t_f] \\
&\doteq \boldsymbol{F}(t_{i,k}, \boldsymbol{z}_{i,k}, \boldsymbol{u}_{\Gamma(i)}, \boldsymbol{p}) = \boldsymbol{0}, && \forall i \in [1..n_e],\ k \in [1..n_c].
\end{aligned}$$

The initial condition is straightforward to transcribe. Eq. (20b) is thus transcribed into Eq. (24b). In the same approximative manner that we only enforced the DAE system at the collocation points, the inequality constraints Eqs. (20c), (20d) are transcribed by only enforcing them at the collocation points. Since we have a collocation point at t_f, the terminal constraints Eq. (20e) are straightforward to transcribe using the corresponding NLP variables. The constraints Eqs. (20c)–(20e) are thus transcribed into Eqs. (24c)–(24e). Note that despite the appearance of the constraint on $\Delta \boldsymbol{u}_n$ in Eq. (24d), it is an inequality constraint of the form Eq. (21d) rather than Eq. (21b).

Finally, Eqs. (24f) and (24g) are added to preserve the inherent coupling of x and $\dot{x}$ and get a continuous trajectory for the state x. The transcription of Eq. (20) into Eq. (24) is thus complete. By solving the NLP Eq. (24), an approximate local optimum to the dynamic optimization problem Eq. (20) may be obtained. Eq. (24) is typically a large but sparse problem, so exploiting sparsity is critical.

6. Modeling and optimization environment

This section outlines the various languages and tools used to generate the simulation and optimization results. The process model and optimization formulation are implemented using the modeling languages Modelica and its optimization extension Optimica [83]. JModelica.org [84] is used to perform the needed simulations and optimizations.

6.1. CasADi

CasADi [85] (**C**omputer **a**lgebra **s**ystem with **A**utomatic **Di**fferentaion) is an open-source, low-level symbolic tool for efficiently computing derivatives using algorithmic differentiation (AD) and is tailored for dynamic optimization. CasADi plays a central role in the dynamic optimization framework of JModelica.org [86]. Once a symbolic representation of Eq. (24) has been created

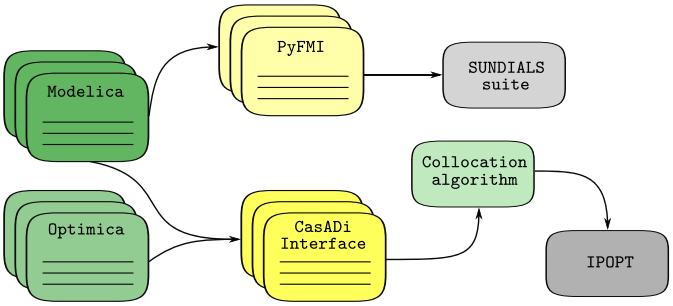

Fig. 2. The JModelica.org toolchain. For simulation purposes, C code is generated based on the Modelica code based on the FMI standard. The user interacts with C code via the Python-based interface PyFMI, which connects the model with numerical integrators from the SUNDIALS suite. For optimization purposes, the Modelica and Optimica code is transferred to CasADi Interface, which serves as an interface to JModelica.org's collocation-based algorithm. The collocation algorithm transcribes the optimization problem into an NLP, which then is solved by IPOPT.

using CasADi constructs, the needed derivatives are efficiently and conveniently obtained and sparsity patterns are preserved.

CasADi utilizes two different graph representations for symbolic expressions. The first is a scalar representation, called SX, where all atomic operations are scalar-valued, as is typical for AD tools. The second is a sparse matrix representation, MX, where all atomic operations instead are multiple-input, multiple-output matrix-valued. The MX representation is more general and allows for efficient, especially in terms of memory, representation of high-level operations, such as matrix multiplication and function calls. On the other hand, the SX representation offers faster computations by reducing overhead and performing additional symbolical simplifications.

6.2. JModelica.org

JModelica.org [84] is an open-source platform for simulation- and optimization-based analysis of large-scale physical models described by Modelica. The main component of JModelica.org is its Modelica and Optimica compiler, which is implemented in Java. Besides performing the usual compiler operations, such as type analysis, it also performs symbolic transformations of the Modelica model, such as index reduction [87] for high-index DAE systems, causalization [88], and analytic solution of trivial equations. The compiler then generates code for two separate toolchains: one for simulation and one for optimization, as illustrated in Fig. 2. The

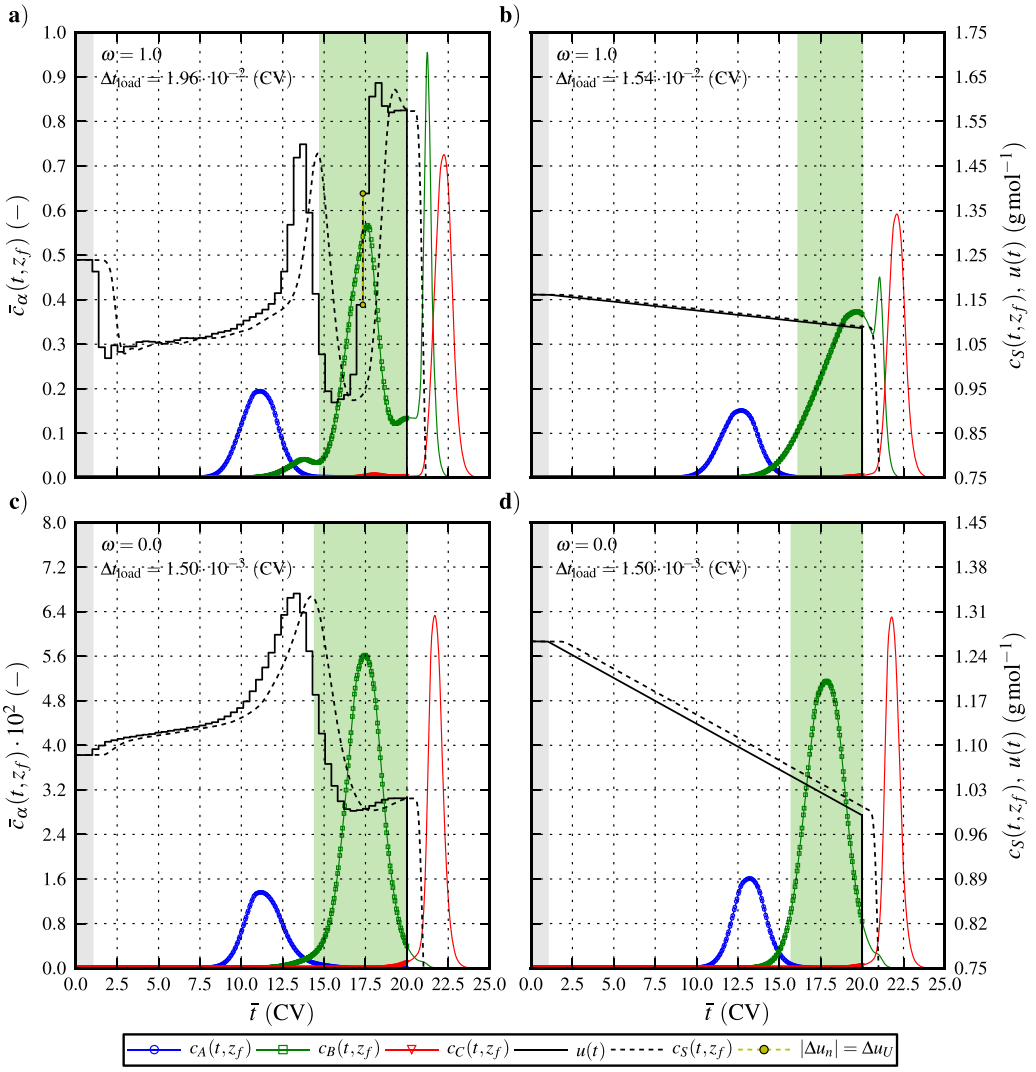

Fig. 3. Pareto optimal state and control trajectories, where $c_\alpha(t, z_f)$ and $\forall \alpha \in \{A, B, C\}$ is normalized with 2.0×10^{-3} (mol m^{-3}), for $X_{B,L} = 0.99$, $R = 5.0 \times 10^{-2}$ and $\omega \in \{0.0, 1.0\}$. Markers indicate the solution at the Radau collocation points and solid and dashed lines the corresponding simulated response. The shaded areas indicate the fractionation interval endpoints, $[\tau_0, \tau_0 + \Delta\tau]$, and that of the initial load and wash.

user interacts with all the different JModelica.org modules using the scripting language Python.

For simulation purposes, the compiler generates C code according to the Functional Mock-Up Interface (FMI) standard [89], essentially transforming the DAE system into a system of ODEs. The generated C code is then imported into PyFMI,[1] which connects it with various numerical integrators via Assimulo [90], in particular the SUNDIALS suite [91].

For optimization purposes, the compiler instead communicates with JModelica.org's CasADi Interface [92]. CasADi Interface serves as an interface between Modelica and Optimica code and numerical optimization algorithms, by providing a symbolic representation of a dynamic optimization problem, based on CasADi's MX graphs, which then can be used to compute the derivatives needed to numerically solve the optimization problem. This representation is then used by JModelica.org's collocation-based algorithm to transcribe the dynamic optimization problem into Eq. (24), which is implemented in Python using CasADi's Python front-end. The collocation algorithm is described in Section 5.2.

The MX representation of the dynamic optimization problem in CasADi Interface is not suitable for Eq. (18), where an SX representation is more suitable due to the scalar nature of the equations. Thus, the MX representation is converted into an SX representation on the fly, which then is used to create an MX representation of Eq. (24), by exploiting the repetitive structure of the NLP in each collocation point using function calls. This approach of mixing MX and SX graphs has been crucial in this study due to the model size, by providing a suitable trade-off between memory consumption and execution speed. After the construction of the NLP is completed, it is solved using CasADi's interface to IPOPT [38], with derivative and sparsity information provided by CasADi. IPOPT is an open-source primal-dual interior point method for numerical solution of sparse NLPs of the form Eq. (21). In this paper, we use the sparse linear solver MA57 from HSL [93] to solve the linearized KKT system in each iteration of IPOPT.

7. Results and discussion

As outlined in Section 4, two inherently different optimal control strategies are considered and the discrepancy lies in whether Eq. (18) is augmented with the CSS periodicity constraints (13) or not. Moreover, in order to assess the performance of the general elution trajectories governed by the *optimal control strategy I*, these were benchmarked with that of the conventional linear trajectories governed by:

$$u_{\text{lin}}(t) = u_{\text{lin},0} + \left[u_{\text{lin},f} - u_{\text{lin},0}\right]\left(\frac{t - t_{\text{lin},0}}{t_f - t_{\text{lin},0}}\right), \tag{25}$$

where $t_{\text{lin},0} = t_0 + \Delta t_{\text{load}} + \Delta t_{\text{wash}}$ defines the onset of the elution mode, Δt_{wash} is the wash horizon and $(u_{\text{lin},0}, u_{\text{lin},f}) \in \mathbb{R}^2$ are the time-invariant optimization parameters. For the benchmark investigation, an analogous optimal control problem was considered where the quadratic penalty on Δu in Eq. (18a) was removed and bounds on the aforementioned parameters was introduced.

The remainder of this section is divided into three subsections, where the NLP transcription specifics are outlined in Section 7.1 and the open-loop solutions governed by the *optimal control strategy I* and *II* are presented in Sections 7.2 and 7.3, respectively.

[1] https://pypi.python.org/pypi/PyFMI.

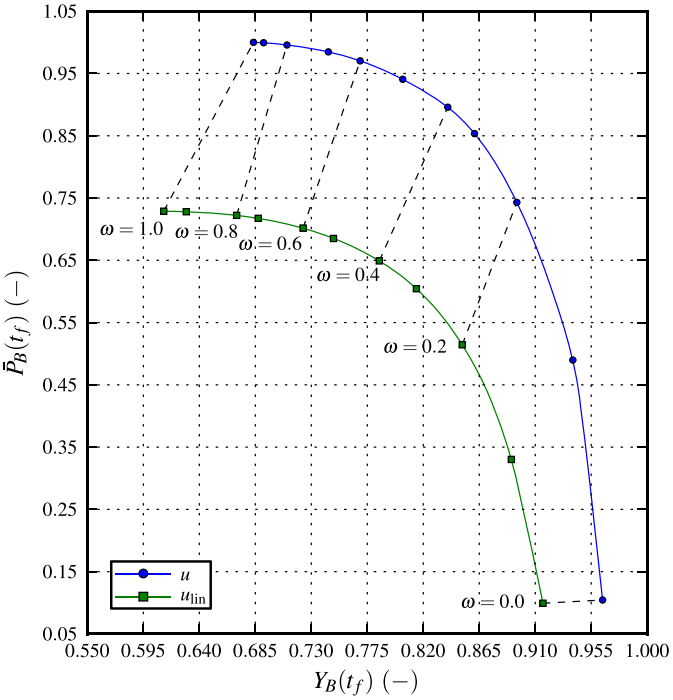

Fig. 4. Pareto optimal fronts generated with the zero-order hold elution trajectory, u, and the conventional linear trajectory, u_{lin}, for $X_{B,L} = 0.99$ and $\omega \in [0.0, 1.0]$.

7.1. NLP transcription specifics and initialization

In this study, the first- and second-order spatial derivative of the concentrations in the convection–diffusion equation (1), which governs the dynamics of the mobile phase, have been approximated using a WENO scheme of fifth order with $n_v = 25$ finite volume elements. The number of finite volume elements is a compromise between accuracy and computational complexity, and is experimentally verified to give adequate representation of the dispersion. Unless otherwise stated, the temporal horizon was discretized with $n_e = 2 \times 10^2$ finite elements with two Radau collocations points in each element and a zero-order hold control discretization with $N_u = 50$ pieces was adopted. Accordingly, the resulting NLP (24) has approximately 2×10^5 variables and was solved on an Ubuntu 12.04 computer with an Intel® Core™ i7-2600 Quad Processor @3.40 GHz. Revision [6718] of JModelica.org was used together with version 3.11.8 of IPOPT with the linear solver MA57. The NLP constrained by the DAE system dynamics was solved to a tolerance of 1×10^{-13} and a total CPU time of approximately 0.75 h.

The collocation method used corresponds to a fixed-step-size Radau solver. To verify the temporal discretization, the optimal input and parameters are used to simulate the system using CVode from the SUNDIALS suite [91], which is a variable-step-size, backward-differentiation formula solver with error control. Moreover, the performance of numerical optimizers, when solving large-scale nonconvex optimization problems, relies on accurate initial guesses of the solution to the problem as well as the problem being reasonably well scaled numerically. This scaling is performed based on the generated initial guess, which in turn was obtained from simulation under isocratic conditions. Variable scaling has been done using the time-variant linear scaling method described in [86], where a scaling factor is computed for every system variable at every collocation point. Equation scaling has been done using the default procedure in IPOPT. Finally, given the simulated DAE response, scaling and initial guess for the fractionation interval manipulated variables were obtained from optimizing the recovery yield (14), subject to the purity inequality constraint (17), using a

sequential quadratic programming algorithm. Hence, this strategy is analogous to that developed in [5,7].

7.2. Open-loop optimal control strategy I – batch elution operation mode

In order to assess the performance of the general elution trajectories, these were benchmarked with that of the conventional linear trajectories (parameterized by Eq. (25)) by means of solving the bi-level optimal control problem (19) with $q = \Delta t_{\text{load}}$ as optimization variable in the upper level (19a) and 19b)). The lower-level optimal control problem (19c)–(19g)) excluding the CSS periodicity constraints (13) is computed over a fixed temporal horizon of $\forall \bar{t} \in [0.0, 20.0]$. Here $\bar{t} = t(\dot{Q}V_c^{-1})$ is the normalized time in column volumes (CV). The specifications in the optimization problem are $X_{B,L} = 9.9 \times 10^{-1}$, $\Delta u_U = 2.5 \times 10^{-1}$, $u_m \in [5.0 \times 10^{-2}, 2.0]$ and $t_f \in [2.0, 5.0] \times 10^1$. The resulting optimal state and control trajectories for $\omega \in \{0.0, 1.0\}$ are depicted in Fig. 3. The optimization and verification simulation results, where markers indicate the solution at the Radau collocation points and solid and dashed lines the corresponding simulated response, are practically identical. The initial control, u_1, is constrained to be constant over the load and the subsequent wash horizon $[t_0,\ t_0 + \Delta t_{\text{load}} + \Delta t_{\text{wash}}]$ where $\Delta t_{\text{wash}} = 1.0$ (CV), it is however considered as a manipulated variable. Although not considered in the open-loop optimal control problem, the control signal is prescribed a constant value of 5.0×10^{-1} (g mol^{-1}) during 5.0 CV regeneration in order to elute the most retained component.

The optimal state and control trajectories illustrated in Fig. 3 show a clear distinction in the system response generated with u and u_{lin}, respectively. As expected from the generic HIC elution mode, u_{lin} and hence the optimal modifier concentration is strictly decreasing in $[t_{\text{lin},0},\ t_f]$ in order to increase hydrophobicity, see Fig. 3b and d. Governed by the individual component adsorption affinities, components $\alpha \in \{A, B, C\}$ are gradually separated as they traverse the column. Contrarily, the modifier concentration is freely controlled with the general elution trajectories, u, shown in Fig. 3a and c. It is evident that the additional degrees of freedom introduced significantly promotes the recovery yield, $Y_B(t_f)$, of the intermediately eluting component B. Moreover, the solvent strength is gradually increasing until the lower optimal fractionation time, τ_0, is reached. At the onset of the fractionation interval, the slope of the elution trajectory changes sign, and the decreasing solvent strength causes the target component to desorb and ultimately to elute. Finally, the slope of the control trajectory changes sign again within the fractionation interval in order to

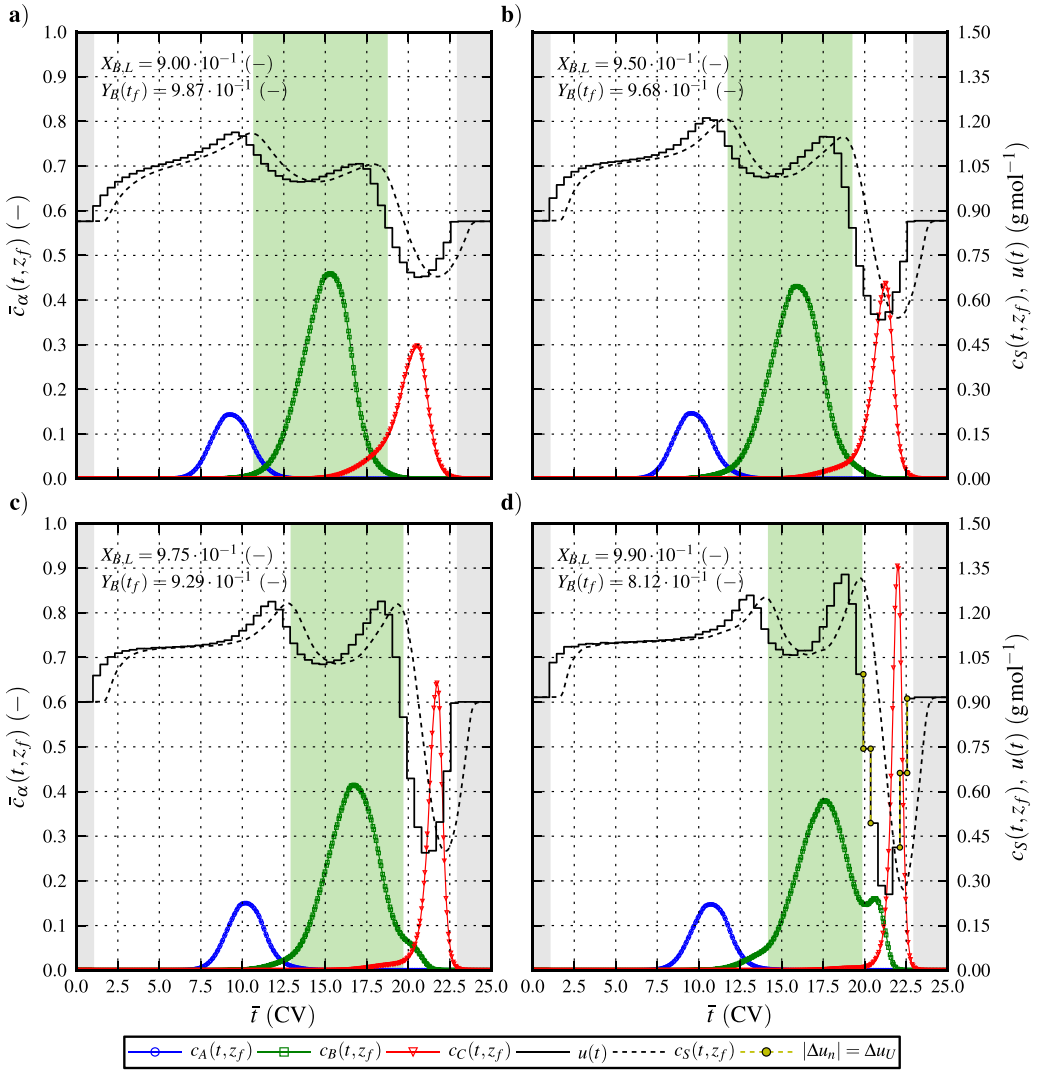

Fig. 5. Optimal CSS elution trajectories, where $c_\alpha(t, z_f)$ and $\forall \alpha \in \{A, B, C\}$ is normalized with 1.75×10^{-3} (mol m^{-3}), for $X_{B,L} \in \{0.90, 0.95, 0.975, 0.99\}$ and $R = 5.0 \times 10^{-2}$. Markers indicate the solution at the Radau collocation points and solid and dashed lines the corresponding simulated response. The shaded areas indicate the fractionation interval endpoints, $[\tau_0,\ \tau_0 + \Delta\tau]$, and those of the initial load and wash and the terminal re-equilibration.

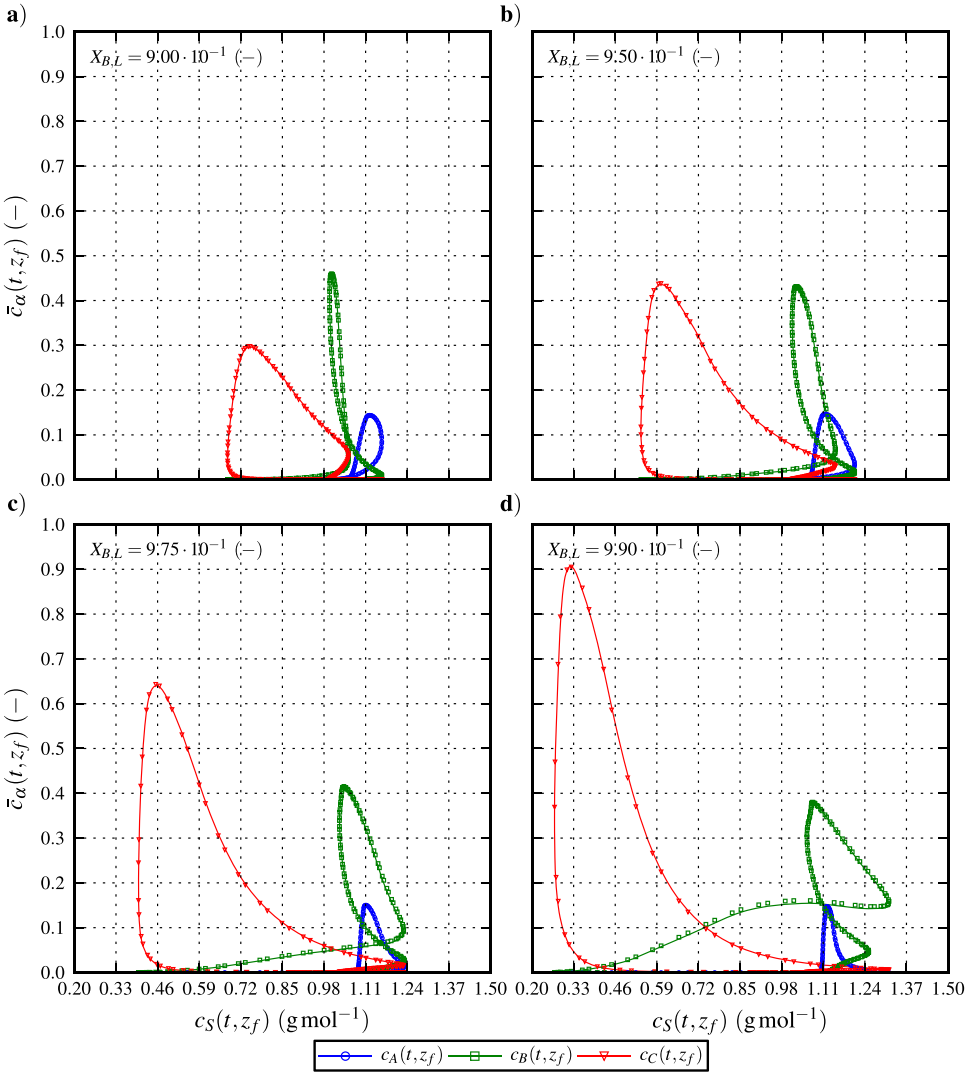

Fig. 6. Phase plane portraits illustrating the state trajectories $c_\alpha(t, z_f)$ and $\forall \alpha \in \{A, B, C\}$ as a function of the modifier concentration $c_S(t, z_f)$ at $z = z_f$ and $\forall t \in [t_0, t_f]$. Markers indicate the solution at the Radau collocation points and solid and dashed lines the corresponding simulated response.

prevent the most retained component to desorb. It is noteworthy that the upper fractionation interval endpoint coincide with the final time. Consequently, when considering the *open-loop optimal control strategy I*, the optimization variable $\Delta\tau$ can safely be omitted in the lower-level DOP (19c)–(19g) and can be replaced by $(t_f - \tau_0)$.

The optimal open-loop controlled trajectories depicted in Fig. 3 for $\omega \in \{0.0, 1.0\}$ comprise the solutions of the single objective optimal control problems for each criterion in Eq. (16). The associated bi-objective Pareto optimal fronts are shown in Fig. 4. It is evident that the general elution trajectories, u, outperform the linear trajectories, u_{lin}, in terms of both objectives. Especially, for $\omega = 1.0$ the maximum productivity obtained with u is approximately 37% higher than that for u_{lin}. It is also noteworthy that the maximum productivity obtained with u is associated with a significantly higher recovery yield. This is explained by the improved resolution capability of the zero-order hold control, i.e. the ability to remove impurity (component A and C) trajectories spanning inside the fractionation interval and causing degraded target component purity as a result. Consequently, this allows for the fractionation interval to span over a wider temporal horizon which significantly enhances the captured amount of the target component. The insights gained from analyzing Fig. 4 clearly motivate the scope of this study, and the tools and methods developed here for solving the optimal control problem (18).

The dependency of $P_B(t_f)$ and $Y_B(t_f)$ on the optimization variable Δt_{load} shows that $Y_B(t_f)$ is strictly decreasing as $\Delta t_{\text{load}} \to \Delta t_{\text{load},U}$ whereas $P_B(t_f)$ exhibits a concave behavior. This was to be expected since maximizing $Y_B(t_f)$ (which is time-invariant) implies injecting a minimal column load, and hence, Δt_{load} is constrained by its lower boundary, and the gain in $Y_B(t_f)$ for u is therefore only moderate (cf. Fig. 3c and d). An analogous behavior was recently observed in [94]. In that study, the final time, t_f, was incorporated in the bi-level optimal control problem formulation. As expected from introducing additional degrees of freedom, both the recovery yield and the production rate were enhanced, however more importantly, the general elution trajectories still outperformed the linear trajectories in terms of both objectives.

7.3. *Open-loop optimal control strategy II – cyclic-steady-state operation mode*

So far, we have shown the optimal open-loop controlled elution trajectories for the control strategy excluding the CSS periodicity constraints (13). This section is therefore devoted to demonstrate optimal control of the comprehensive cyclic-steady-state

formalism. As outlined in Section 4.1, computation of CSS solutions over the temporal horizon $t \in [t_0, t_f]$ requires that the open-loop optimal control problem (18) is augmented with the periodicity criteria governing that the state at the initial time is retained at the end of the cycle. The optimal state and control trajectories for $\omega = 0.0$ and $X_{B,L} \in \{0.90, 0.95, 0.975, 0.99\}$ that conform to the periodicity constraints over a fixed temporal horizon of $\forall \bar{t} \in [0.0, 25.0]$ are displayed in Fig. 5. Here, the initial control, u_1, is constrained to be constant over the load and the subsequent wash horizon $[t_0, t_0 + \Delta t_{\text{load}} + \Delta t_{\text{wash}}]$, however freely controlled. Moreover, the control in the final re-equilibration horizon $[t_f - \Delta t_{\text{eq}}, t_f]$, where $\Delta t_{\text{eq}} = 2.0$ (CV), is prescribed the constant value of u_1 through the periodicity criterion defined in Eq. (13d).

The optimal open-loop controlled trajectories depicted in Fig. 5 shows that the solvent strength is gradually increasing until the lower optimal fractionation time, τ_0, is reached. Subsequently, the slope of the control trajectory changes sign within the fractionation interval in order to prevent the most retained component to desorb. At the upper fractionation interval endpoint, the control trajectory drastically drops in order to completely elute component C, and to fulfill Eq. (13a), before returning to the initial control level. For these reasons, the upper endpoint of the fractionation interval, $(\tau_0 + \Delta\tau)$, does not coincide with the that of the temporal horizon, as was the case for the optimal control trajectories shown in Fig. 3. It is also evident from Fig. 5 that there is a high intercorrelation between the shape of the zero-order hold control and the fractionation interval endpoints. Hence, the optimal fractionation interval endpoints coincide with the location of the zero temporal derivative of the eluent concentration at the outlet, i.e. $\partial c_S(t, z_f)/\partial t := 0$. This phenomenon is expected since the local eluent concentration at the outlet, $c_S(t, z_f)$, rather than the optimal control prescribed at the inlet, ultimately governs prospects for fractionation. Moreover, by comparing the elution profiles depicted in Fig. 5 for different lower purity requirements $X_{B,L} \in \{0.90, 0.95, 0.975, 0.99\}$ it is evident that the fractionation interval spans over a more narrow temporal horizon for more stringent purity requirements with degraded recovery yield as a result. Additionally, the onset of the fractionation interval is slightly shifted towards higher elution volumes as $X_{B,L} \to 1.0$. Consequently, the most retained component has to be eluted during a shorter time period, and hence, the difference of the piecewise constant controls, Δu_n, are significantly larger in the temporal horizon for $t > \tau_0 + \Delta\tau$.

Fig. 6 presents an alternative view of the state variable CSS dynamics where $c_\alpha(t, z_f)$ and for $\alpha \in \{A, B, C\}$ are depicted as a function of the modifier concentration $c_S(t, z_f)$. The cyclic-steady-state solutions can be easily identified in the phase plane portraits, and it is evident that the projected state trajectories depicted in Fig. 5 are closed curves. This implies that all states conform to the CSS periodicity constraints over the temporal horizon $[t_0, t_f]$. By these means, the *optimal control strategy II* imposes adequate retention time repeatability by conditioning the column to the initial modifier concentration and by enforcing complete elution of the most retained component prior to the subsequent injection.

As was observed from analyzing Fig. 5, a clear performance decrease in terms of recovery yield was obtained when enforcing more stringent purity constraints. In order to assess the impact of $X_{B,L}$ on the Pareto optimal solutions that conform to the CSS periodicity constraints, the bi-level optimal control problem (19), introducing $t_f \in [1.0, 5.0] \times 10^1$ as optimization variable in the upper level (19a–19b)), was repeatedly solved for $X_{B,L} \in \{0.95, 0.975, 0.99\}$. The resulting Pareto optimal fronts for $\omega \in [0.0, 1.0]$ are depicted in Fig. 7 for comparison purposes. It is evident that both $Y_B(t_f)$ and $P_B(t_f)$ strictly decrease for all $\omega \in [0.0, 1.0]$ in order to fulfill a more stringent constraint placed on the target component purity. Moreover, the discrepancy between the Pareto optimal fronts increases as $\omega \to 1.0$. The associated Pareto optimal

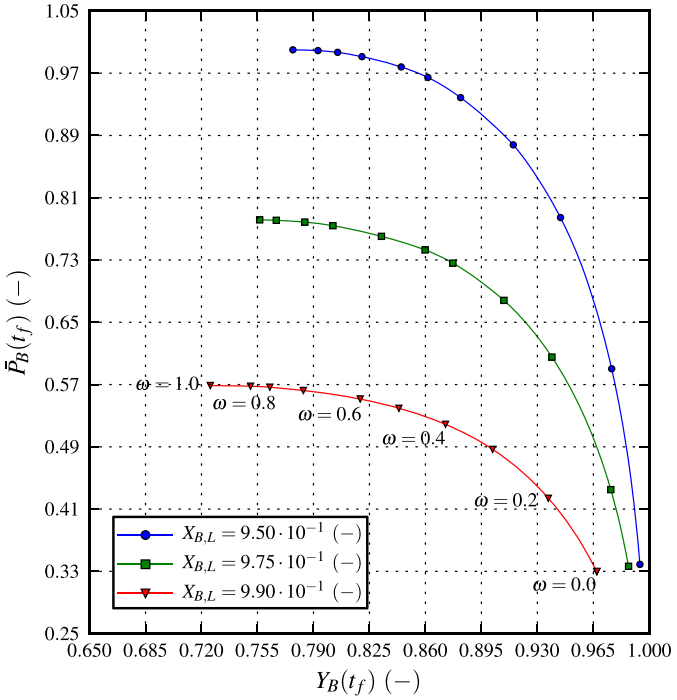

Fig. 7. Pareto optimal fronts generated with the zero-order hold elution trajectory, that conform to the CSS periodicity constraints, for $X_{B,L} \in \{0.95, 0.975, 0.99\}$ and $\omega \in [0.0, 1.0]$.

control and state trajectories are depicted in Fig. 8 for $\omega \in \{0.0, 1.0\}$ and $X_{B,L} \in \{0.95, 0.975\}$. The value of the optimization variable t_f decreases as $\omega \to 1.0$, which originates from the inverse dependence of $P_B(t_f)$ on t_f in Eq. (15). Consequently, there is a clear distinction between the associated Pareto optimal state and control trajectories. Specifically, there is no prominent change in the slope of the elution trajectories within the fractionation interval for $\omega = 0.0$. Contrarily, the optimal control trajectories exhibit a clear "*M-shaped*" dependence in this region for the case of $\omega = 1.0$ in order to improve the resolution, i.e. prohibiting that impurity (component A and C) trajectories span inside the fractionation interval, in a significantly shorter cycle time.

7.3.1. *Penalty on the difference of the zero-order hold controls*

This section is devoted to demonstrate the influence of the quadratic penalty on the difference of the zero-order hold controls that is augmented to the cost function (16). It is noteworthy that a value of the penalty factor, R, larger than zero will always yield a more smooth control trajectory and will always give rise to a performance decrease. Moreover, prescribing an infinitely high value to R will result in a constant elution trajectory given that isocratic conditions yield a feasible solution, i.e. the target component purity constraint is fulfilled.

In order to assess the impact of R on the recovery yield, the optimal control problem (18) was solved for $R \in \{0.0, 0.01, 0.25, 0.50\}$. The resulting optimal state and control trajectories are depicted in Fig. 9 for comparison purposes. Specifically, the unpenalized control shown in Fig. 9a is associated with $Y_B(t_f) = 8.19 \times 10^{-1}$ and the most penalized control depicted in Fig. 9d is associated with $Y_B(t_f) = 7.54 \times 10^{-1}$. However, it is noteworthy that there is only a moderate decrease in the recovery yield for values of $R \leq 0.05$ (see also Fig. 5d).

The solution of the open-loop optimal control problem (18) yields trajectories that lie on the boundary of the feasible region, i.e. the resulting purity equals its lower requirement. Consequently, the open-loop controlled system is unable to cope with process

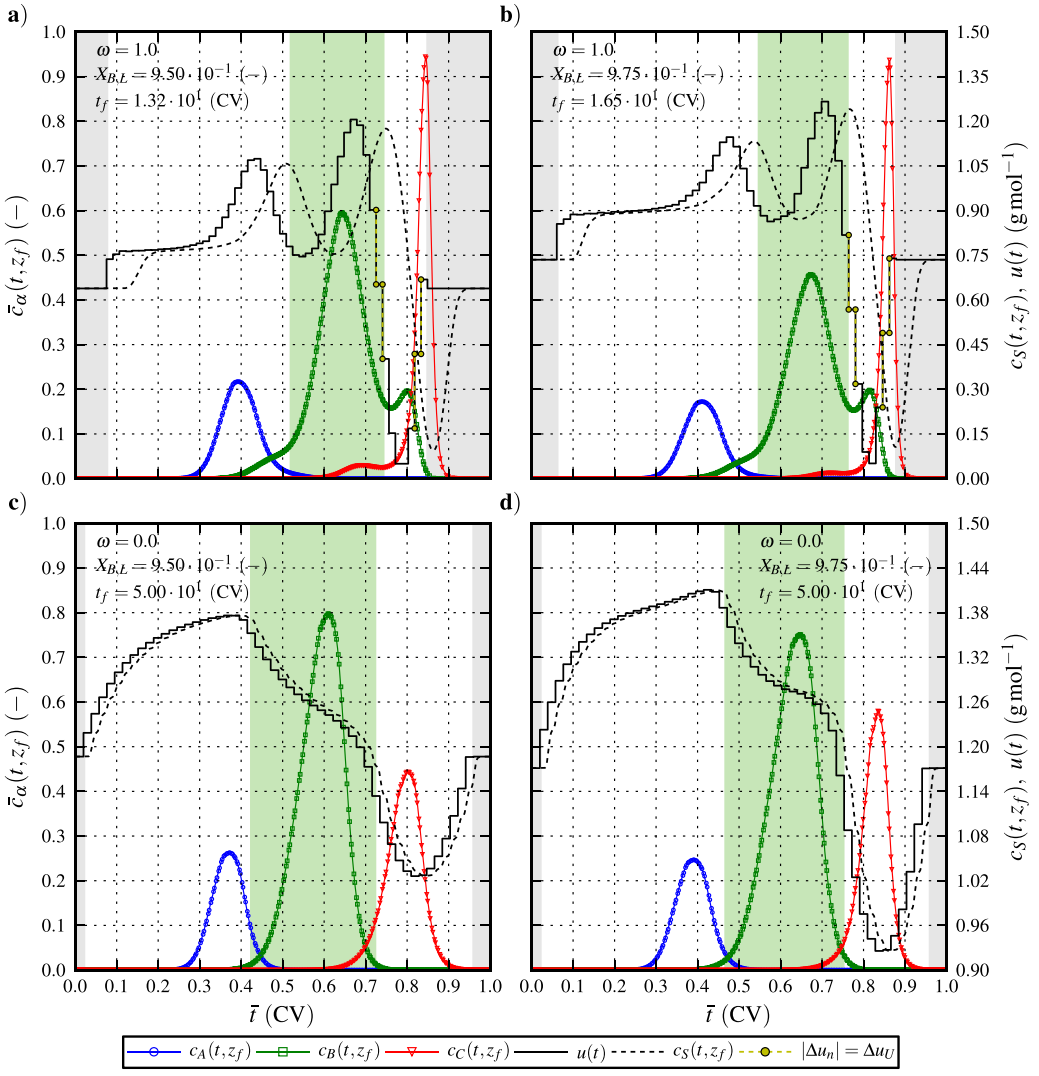

Fig. 8. Pareto optimal CSS elution trajectories, where $c_\alpha(t, z_f)$ and $\forall \alpha \in \{A, B, C\}$ is normalized with 1.75×10^{-3} (mol m^{-3}), for $X_{B,L} \in \{0.95, 0.975\}$, R = 5.0×10^{-2} and $\omega \in \{0.0, 1.0\}$. Markers indicate the solution at the Radau collocation points and solid and dashed lines the corresponding simulated response. The shaded areas indicate the fractionation interval endpoints, $[\tau_0, \tau_0 + \Delta\tau]$, and that of the initial load and wash.

variability and to surmount this shortcoming calls for the formulation of a robust counterpart problem [95]. The comprehensive theoretical background in extending the open-loop optimal control problem (18) with its robust counterpart formulation was recently developed in [96]. In that study, a deterministic robustified safety margin (or back-off term) [97–99] was used to augment the purity constraint and R was introduced as an optimization variable in the robust counterpart problem. Hence, the robustification of the open-loop controlled system implies compromising high penalties on the change in the zero-order hold control, yielding optimal solutions with low sensitivity to uncertainty, however, to the expense of an overall lower performance. As robustness is of the highest importance in biopharmaceutical process industry, see e.g. the *process analytical technology* (PAT) and *quality-by-design* (QbD) guidelines [100–102] published by the United States Food and Drug Administration (US FDA), this motivates the inclusion of the term penalizing Δu_n and $\forall n \in [1..N_u - 1]$ in the cost function (16).

7.3.2. Zero-order hold control signal update frequency

This section is devoted to demonstrate the influence of the zero-order hold control signal update frequency, i.e. the number of control levels N_u used in piecewise-constant control parameterization. In order to assess the impact of N_u on the recovery yield, the optimal control problem (18) was solved for $N_u \in \{25, 75, 100, 150\}$ and R was prescribed a value of 1.0×10^{-2} in order to reduce the impact of the quadratic penalty on the difference of the zero-order hold controls. The resulting optimal state and control trajectories are depicted in Fig. 10 for comparison purposes. It is evident that a higher value of N_u yields a performance increase, however, there is only a moderate increase in $Y_B(t_f)$ for values of $N_u > 75$. Consequently, the performance increase for a higher zero-order hold control signal update frequency, introducing more degrees of freedom to optimal control problem (18), is restricted by the complex system dynamics associated with long time delays and spatially distributed properties.

The performance increase to be expected when increasing N_u is highly system dependent, and originates from the upstream mixing unit residence time. Specifically, a large mixing unit residence time ($V_{\text{mix}}/\dot{Q}$) will highly influence the smoothness of the modifier concentration, $c_S(t, z_0)$, profile prescribed at the column inlet (see Eq. (2)). In the extreme case when the HPLC system is operated under a low volumetric flow rate and when $V_{\text{mix}} \geq V_c$, the rectangular stairs of the control input (with high-frequency update) is lost in the first-order system dynamics governed by the mixing unit (see Eq. (4)). As was previously discussed, it is the local eluent concentration inside the column, $c_S(t, z)$ and $\forall z \in [z_0, z_f]$, rather then

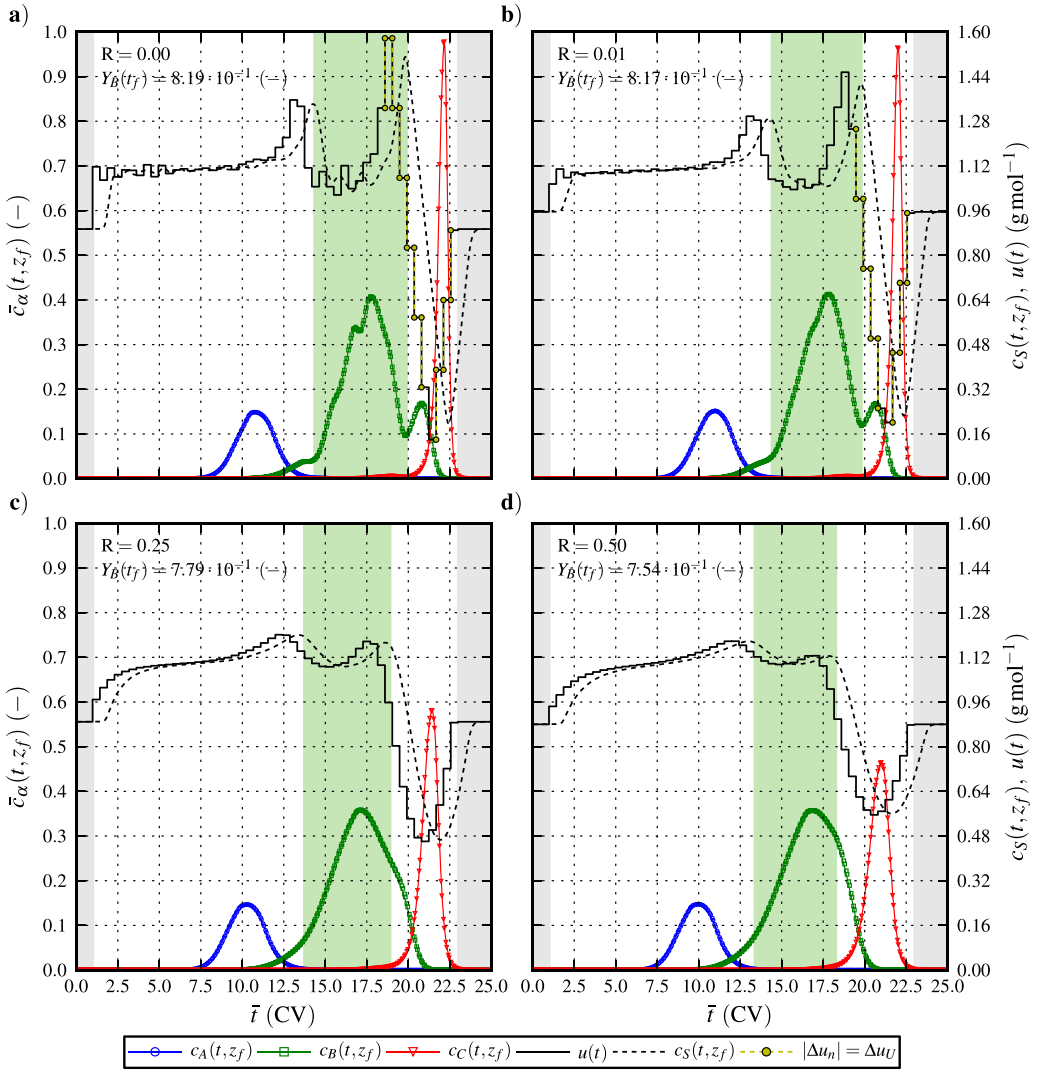

Fig. 9. Optimal CSS elution trajectories, where $c_\alpha(t, z_f)$ and $\forall \alpha \in \{A, B, C\}$ is normalized with 2.25×10^{-3} (mol m^{-3}), for $X_{B,L} = 0.99$ and R $\in \{0.0, 0.1, 0.25, 0.50\}$. Markers indicate the solution at the Radau collocation points and solid and dashed lines the corresponding simulated response. The shaded areas indicate the fractionation interval endpoints, $[\tau_0, \tau_0 + \Delta\tau]$, and those of the initial load and wash and the terminal re-equilibration.

the optimal control prescribed at the inlet to the mixing unit, that ultimately governs prospects for fractionation and the maximum amount of target component captured. Hence, in order to preserve the additional degrees of freedom provided by the zero-order hold control trajectory, it is essential to minimize the HPLC system volume upstream the column. The experimental validation and the practical aspects in realizing the general elution trajectory will be considered in a follow-up study.

8. Concluding remarks

Chromatography is an essential downstream process operation to isolate a high-purity target component from a multi-component mixture in the pharmaceutical and biochemical industries. The removal of closely related product impurities in preparative and industrial scale chromatography separations is specifically challenging and requires both high performance resins and optimized elution mode. Although modulation of the solvent strength during trajectory elution is widely applied in preoperative chromatography, in order to enhance resolution of high complex sample mixtures, it still relies on simpler linear-, concave or convex- and various types of step trajectories. This paper is therefore concerned with the development of a novel open-loop optimal control strategy for HPLC separation processes. However, there is a drastic increase in computational complexity while moving from the conventional elution trajectories, associated with a few degrees of freedom, to the general elution trajectories, parameterized with a large number piecewise constant controls. To efficiently and accurately generate optimal elution trajectories we considered a simultaneous optimization method where both the state and control variables of the original PDE-constrained DOP are fully discretized in the temporal domain using direct local collocation. One of the main contributions of this paper is therefore the established methodology and the computationally efficient framework for open-loop optimal control of batch chromatographic separation processes. It is however noteworthy that the generic methods and tools developed here are applicable to any large-scale optimal control problem constrained by PDEs.

In this study, a weighted sum scalarization method was used to combine the competing objective functions of recovery yield and productivity into a single performance index. This allowed the use of deterministic NLP routines and ensured an accurate and efficient Pareto set generation. It is noteworthy that optimizing productivity yields the formulation of a minimal time

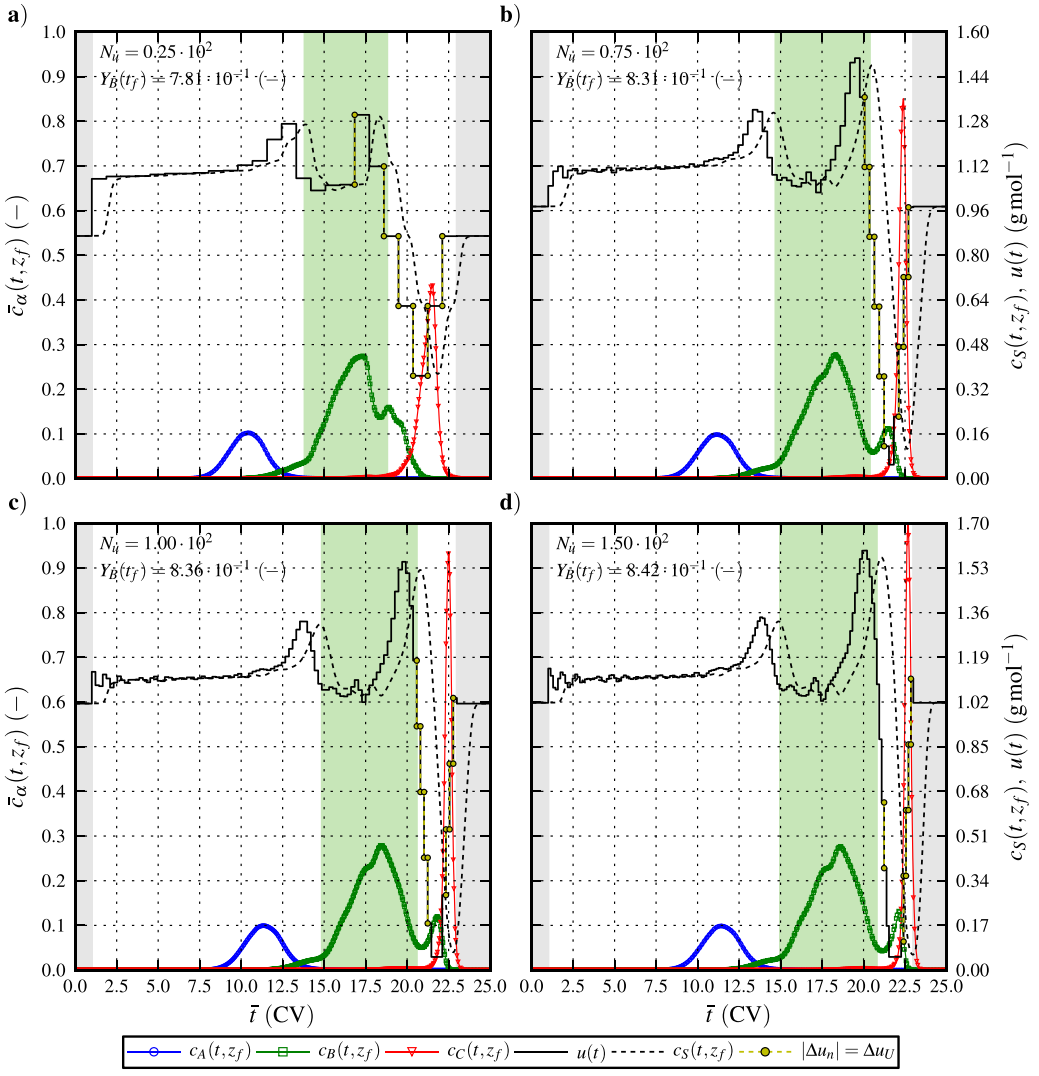

Fig. 10. Recovery yield optimal CSS elution trajectories, where $c_\alpha(t, z_f)$ and $\forall \alpha \in \{A, B, C\}$ is normalized with 1.75×10^{-3} (mol m^{-3}), for $X_{B,L} = 0.99$ and $N_u \in \{25, 75, 100, 150\}$. Markers indicate the solution at the Radau collocation points and solid and dashed lines the corresponding simulated response. The shaded areas indicate the fractionation interval endpoints, $[\tau_0, \tau_0 + \Delta\tau]$, and those of the initial load and wash and the terminal re-equilibration.

control problem which was not computationally tractable due to the large-scale and nonlinear PDE-constrained dynamics. However, computational tractability was obtained by casting the open-loop optimal control problem in the framework of bi-level optimal control where the upper level concerns the set of time-variant optimization variables, and the DOP is considered in the lower level. The lower-level DOP constrained by the system dynamics was transcribed into a sparse NLP using direct collocation, which was then solved by IPOPT supplied with the first- and second-order derivatives of the NLP functions computed using CasADi's algorithmic differentiation while preserving sparsity. The fully-discretized NLP formulation and interior-point solver has been found to be efficient and reliable for the optimal control problem of the batch HPLC process considered.

The advantages of the optimal control methodology were illustrated through the solution of a specific challenging ternary complex mixture separation problem of insulin analogs, with the intermediately eluting component as the target, by hydrophobic interaction chromatography. Moreover, two inherently different optimal control strategies were considered and the difference lies in whether the optimal control problem is augmented with the cyclic-steady-state periodicity constraints or not. A key result of this study is that the general elution trajectories nonconforming to the CSS periodicity constraints outperformed the conventional linear trajectories both in terms of recovery yield and productivity. Especially, a significant increase in maximum productivity was obtained for the open-loop controlled trajectories. This was explained by the improved resolution capability of the zero-order hold control, i.e. the ability to remove impurity trajectories spanning inside the fractionation interval and causing degraded target component purity as a result. Consequently, this allowed for the fractionation interval to span over a wider temporal horizon and significantly enhanced the captured amount of the target component.

It was also demonstrated that the optimal control problem augmented with the cyclic-steady-state periodicity constraints enabled control over the column regeneration and re-equilibration modes, and consequently enabled minimization of those time periods while fulfilling the constraint imposed on purity of the target component fractionation. The results obtained showed that there is a high intercorrelation between the shape of the zero-order hold control and the fractionation interval endpoints. Specifically, the optimal fractionation interval endpoints coincided with the location of the zero temporal derivative of the eluent concentration at the outlet of the column. This phenomenon is governed

by the system's spatially distributed properties. In this context, the assessment of the zero-order hold control signal update frequency showed that the performance increase for a higher update frequency was restricted by the complex system dynamics associated with long time delays and spatially distributed properties. The performance increase to be expected is highly system dependent, and originates from the upstream mixing unit residence time. Specifically, a large mixing unit residence time will highly influence the smoothness of the elution trajectory, and in the limiting case, the rectangular stairs of the control input (with high-frequency update) is lost in the first-order system dynamics governed by the mixing unit. It is therefore essential to minimize the HPLC system volume upstream the column in order to preserve the additional degrees of freedom provided by the zero-order hold control trajectory.

Acknowledgments

The authors acknowledge the support of the strategic innovation program Process Industrial IT and Automation (SIO–PiiA) and the LCCC Linnaeus Center and the eLLIIT Excellence Center at Lund University.

References

[1] C. Ündey, S. Ertunç, T. Mistretta, B. Looze, Applied advanced process analytics in biopharmaceutical manufacturing: challenges and prospects in real-time monitoring and control, J. Process Control 20 (9) (2010) 1009–1018, http://dx.doi.org/10.1016/j.jprocont.2010.05.008.
[2] A. Jungbauer, Chromatographic media for bioseparation, J. Chromatogr. A 1065 (1) (2005) 3–12, http://dx.doi.org/10.1016/j.chroma.2004.08.162.
[3] E. Wisniewski, E. Boschetti, A. Jungbauer, Biotechnology and biopharmaceutical manufacturing, processing, and preservation, in: K.E. Avis, V.L. Wu (Eds.), in: Drug Manufacturing Technology Series, 2, 1st ed., Interpharm Press, Inc., Buffalo Grove, IL, 1996.
[4] O. Kaltenbrunner, Y. Lu, A. Sharma, K. Lawson, T. Tressel, Risk-benefit evaluation of on-line high-performance liquid chromatography analysis for pooling decisions in large-scale chromatography, J. Chromatogr. A 1241 (0) (2012) 37–45, http://dx.doi.org/10.1016/j.chroma.2012.04.003.
[5] Y. Shan, A. Seidel-Morgenstern, Analysis of the isolation of a target component using multicomponent isocratic preparative elution chromatography, J. Chromatogr. A 1041 (1–2) (2004) 53–62, http://dx.doi.org/10.1016/j.chroma.2004.04.061.
[6] G. Guiochon, A. Felinger, D.G. Shirazi, A.M. Katti, Fundamentals of Preparative and Nonlinear Chromatography, 2nd ed., Academic Press, San Diego, CA, USA, 2006.
[7] B. Sreedhar, A. Wagler, M. Kaspereit, A. Seidel-Morgenstern, Optimal cut-times finding strategies for collecting a target component from overloaded elution chromatograms, Comput. Chem. Eng. 49 (2013) 158–169, http://dx.doi.org/10.1016/j.compchemeng.2012.09.009.
[8] L.R. Snyder, J.W. Dolan, High-Performance Gradient Elution: The Practical Application of the Linear-Solvent-Strength Model, John Wiley & Sons, Inc., Hoboken, NJ, 2007.
[9] F. Gritti, G. Guiochon, Separations by gradient elution: why are steep gradient profiles distorted and what is their impact on resolution in reversed-phase liquid chromatography, J. Chromatogr. A 1344 (2014) 66–75, http://dx.doi.org/10.1016/j.chroma.2014.04.010.
[10] F. Gritti, G. Guiochon, The distortion of gradient profiles in reversed-phase liquid chromatography, J. Chromatogr. A 1340 (2014) 50–58, http://dx.doi.org/10.1016/j.chroma.2014.03.004.
[11] A. Tarafder, L. Aumann, T. Müller-Späth, M. Morbidelli, Improvement of an overloaded, multi-component, solvent gradient bioseparation through multiobjective optimization, J. Chromatogr. A 1167 (1) (2007) 42–53, http://dx.doi.org/10.1016/j.chroma.2007.07.086.
[12] P. Nikitas, A. Pappa-Louisi, K. Papachristos, Optimisation technique for stepwise gradient elution in reversed-phase liquid chromatography, J. Chromatogr. A 1033 (2) (2004) 283–289, http://dx.doi.org/10.1016/j.chroma.2004.01.048.
[13] P. Jandera, Simultaneous optimisation of gradient time, gradient shape and initial composition of the mobile phase in the high-performance liquid chromatography of homologous and oligomeric series, J. Chromatogr. A 845 (1–2) (1999) 133–144, http://dx.doi.org/10.1016/S0021-9673(99)00331-3.
[14] A.P. Schellinger, D.R. Stoll, P.W. Carr, High-speed gradient elution reversed-phase liquid chromatography of bases in buffered eluents: part I. Retention repeatability and column re-equilibration, J. Chromatogr. A 1192 (1) (2008) 41–53, http://dx.doi.org/10.1016/j.chroma.2008.01.062.
[15] A.P. Schellinger, D.R. Stoll, P.W. Carr, High speed gradient elution reversed phase liquid chromatography of bases in buffered eluents: part II. Full equilibrium, J. Chromatogr. A 1192 (1) (2008) 54–61, http://dx.doi.org/10.1016/j.chroma.2008.02.049.
[16] A.P. Schellinger, D.R. Stoll, P.W. Carr, High speed gradient elution reversed-phase liquid chromatography, J. Chromatogr. A 1064 (2) (2005) 143–156, http://dx.doi.org/10.1016/j.chroma.2004.12.017.
[17] A.P. Schellinger, P.W. Carr, Isocratic and gradient elution chromatography: a comparison in terms of speed, retention reproducibility and quantitation, J. Chromatogr. A 1109 (2) (2006) 253–266, http://dx.doi.org/10.1016/j.chroma.2006.01.047.
[18] S.R. Gallant, S. Vunnum, S.M. Cramer, Optimization of preparative ion-exchange chromatography of proteins: linear gradient separations, J. Chromatogr. A 725 (2) (1996) 295–314, http://dx.doi.org/10.1016/0021-9673(95)00909-4.
[19] A. Osberghaus, S. Hepbildikler, S. Nath, M. Haindl, E. von Lieres, J. Hubbuch, Optimizing a chromatographic three component separation: a comparison of mechanistic and empiric modeling approaches, J. Chromatogr. A 1237 (0) (2012) 86–95, http://dx.doi.org/10.1016/j.chroma.2012.03.029.
[20] Y. Shan, A. Seidel-Morgenstern, Optimization of gradient elution conditions in multicomponent preparative liquid chromatography, J. Chromatogr. A 1093 (1–2) (2005) 47–58, http://dx.doi.org/10.1016/j.chroma.2005.07.047.
[21] A. Damtew, B. Sreedhar, A. Seidel-Morgenstern, Evaluation of the potential of nonlinear gradients for separating a ternary mixture, J. Chromatogr. A 1216 (28) (2009) 5355–5364, http://dx.doi.org/10.1016/j.chroma.2009.05.026.
[22] H. Schmidt-Traub, M. Schulte, A. Seidel-Morgenstern, Preparative Chromatography, 2nd ed., Wiley-VCH, Weinheim, 2012.
[23] L.T. Biegler, O. Ghattas, M. Heinkenschloss, B. van Bloemen Waanders, Large-scale PDE-constrained optimization, in: T.J. Barth, M. Griebel, D.E. Keyes, R.M. Nieminen, D. Roose, T. Schlick (Eds.), in: Lecture Notes in Computational Science and Engineering, 30, Springer, Berlin, Heidelberg/NY, USA, 2003, http://dx.doi.org/10.1007/978-3-642-55508-4.
[24] Constrained optimization and optimal control for partial differential equations, in: G. Leugering, S. Engell, A. Griewank, M. Hinze, R. Rannacher, V. Schulz, M. Ulbrich, S. Ulbrich (Eds.), International Series of Numerical Mathematics, vol. 160, Springer, Basel, AG, 2012, http://dx.doi.org/10.1007/978-3-0348-0133-1.
[25] S. Wendl, H. Pesch, A. Rund, On a state-constrained pde optimal control problem arising from ODE-PDE optimal control, in: M. Diehl, F. Glineur, E. Jarlebring, W. Michiels (Eds.), Recent advances in optimization and its applications in engineering, Springer, Berlin, Heidelberg, 2010, pp. 429–438, http://dx.doi.org/10.1007/978-3-642-12598-0_37.
[26] L.T. Biegler, Nonlinear Programming: Concepts, Algorithms, and Applications to Chemical Processes, MOS-SIAM Series on Optimization, Mathematical Optimization Society and the Society for Industrial and Applied Mathematics, PA, USA, 2010.
[27] J. Betts, Practical Methods for Optimal Control and Estimation Using Nonlinear Programming SIAM's Advances in Design and Control, 2nd ed., Society for Industrial and Applied Mathematics, PA, USA, 2010.
[28] M.E. Davis, Numerical Methods and Modeling for Chemical Engineers, 1st ed., John Wiley & Sons, Inc, New York, 1984.
[29] W.E. Schiesser, The Numerical Method of Lines: Integration of Partial Differential Equations, 1st ed., Academic Press, San Diago, 1991.
[30] W. Gao, S. Engell, Iterative set-point optimization of batch chromatography, Comput. Chem. Eng. 29 (6) (2005) 1401–1409, http://dx.doi.org/10.1016/j.compchemeng.2005.02.035.
[31] G. Dünnebier, S. Engell, A. Epping, F. Hanisch, A. Jupke, K.-U. Klatt, H. Schmidt-Traub, Model-based control of batch chromatography, AIChE J. 47 (11) (2001) 2493–2502, http://dx.doi.org/10.1002/aic.690471112.
[32] Y. Kawajiri, L.T. Biegler, Optimization strategies for simulated moving bed and powerfeed processes, AIChE J. 52 (4) (2006) 1343–1350, http://dx.doi.org/10.1002/aic.10736.
[33] D. Nagrath, A. Messac, B.W. Bequette, S.M. Cramer, A hybrid model framework for the optimization of preparative chromatographic processes, Biotechnol. Prog. 20 (1) (2004) 162–178, http://dx.doi.org/10.1021/bp034026g.
[34] B. Sreedhar, A. Damtew, A. Seidel-Morgenstern, Theoretical study of preparative chromatography using closed-loop recycling with an initial gradient, J. Chromatogr. A 1216 (25) (2009) 4976–4988, http://dx.doi.org/10.1016/j.chroma.2009.04.057.
[35] G.-S. Jiang, C.-W. Shu, Efficient implementation of weighted ENO schemes, J. Comput. Phys. 126 (1) (1996) 202–228, http://dx.doi.org/10.1006/jcph.1996.0130.
[36] C.-W. Shu, Essentially non-oscillatory and weighted essentially non-oscillatory schemes for hyperbolic conservation laws, in: A. Quarteroni (Ed.), Advanced Numerical Approximation of Nonlinear Hyperbolic Equations, Vol. 1697 of Lecture Notes in Mathematics, Springer, Berlin, Heidelberg, 1998, pp. 325–432, http://dx.doi.org/10.1007/BFb0096355.
[37] V. John, J. Novo, On (essentially) non-oscillatory discretizations of evolutionary convection-diffusion equations, J. Comput. Phys. 231 (4) (2012) 1570–1586, http://dx.doi.org/10.1016/j.jcp.2011.10.025.
[38] A. Wächter, L.T. Biegler, On the implementation of an interior-point filter line-search algorithm for large-scale nonlinear programming, Math. Program. 106 (1) (2006) 25–57, http://dx.doi.org/10.1007/s10107-004-0559-y.

[39] A. Griewank, Evaluating Derivatives: Principles and Techniques of Algorithmic Differentiation, Society for Industrial and Applied Mathematics, Philadelphia, PA, 2000.
[40] A. Püttmann, S. Schnittert, U. Naumann, E. von Lieres, Fast and accurate parameter sensitivities for the general rate model of column liquid chromatography, Comput. Chem. Eng. 56 (0) (2013) 46–57, http://dx.doi.org/10.1016/j.compchemeng.2013.04.021.
[41] J.P.B. Mota, J.M.M. Araújo, Single-column simulated-moving-bed process with recycle lag, AIChE J. 51 (6) (2005) 1641–1653, http://dx.doi.org/10.1002/aic.10426.
[42] J.M.M. Araújo, R.C.R. Rodrigues, J.P.B. Mota, Use of single-column models for efficient computation of the periodic state of a simulated moving-bed process, Ind. Eng. Chem. Res. 45 (15) (2006) 5314–5325, http://dx.doi.org/10.1021/ie051108w.
[43] J.M.M. Araújo, R.C.R. Rodrigues, J.P.B. Mota, Optimal design and operation of a certain class of asynchronous simulated moving bed processes, J. Chromatogr. A 1132 (1–2) (2006) 76–89, http://dx.doi.org/10.1016/j.chroma.2006.07.016.
[44] J.P.B. Mota, J.M.M. Araújo, R.C.R. Rodrigues, Optimal design of simulated moving-bed processes under flow rate uncertainty, AIChE J. 53 (10) (2007) 2630–2642, http://dx.doi.org/10.1002/aic.11281.
[45] P. Nestola, R.J.S. Silva, C. Peixoto, P.M. Alves, M.J.T. Carrondo, J.P.B. Mota, Robust design of adenovirus purification by two-column, simulated moving-bed, size-exclusion chromatography, J. Biotechnol. (2015), http://dx.doi.org/10.1016/j.jbiotec.2015.01.030.
[46] T. Barz, S. Kuntsche, G. Wozny, H. Arellano-Garcia, An efficient sparse approach to sensitivity generation for large-scale dynamic optimization, Comput. Chem. Eng. 35 (10) (2011) 2053–2065, http://dx.doi.org/10.1016/j.compchemeng.2010.10.008.
[47] M.E. Lienqueo, A. Mahn, J.C. Salgado, J.A. Asenjo, Current insights on protein behaviour in hydrophobic interaction chromatography, J. Chromatogr. B 849 (1–2) (2007) 53–68, http://dx.doi.org/10.1016/j.jchromb.2006.11.019.
[48] A. Mahn, M.E. Lienqueo, J.A. Asenjo, Optimal operation conditions for protein separation in hydrophobic interaction chromatography, J. Chromatogr. B 849 (1-2) (2007) 236–242, http://dx.doi.org/10.1016/j.jchromb.2006.09.013.
[49] K.-U. Klatt, F. Hanisch, G. Dünnebier, S. Engell, Model-based optimization and control of chromatographic processes, Comput. Chem. Eng. 24 (2–7) (2000) 1119–1126, http://dx.doi.org/10.1016/S0098-1354(00)00492-0.
[50] S.K. Hansen, E. Skibsted, A. Staby, J. Hubbuch, A label-free methodology for selective protein quantification by means of absorption measurements, Biotechnol. Bioeng. 108 (11) (2011) 2661–2669, http://dx.doi.org/10.1002/bit.23229.
[51] F. Allgöwer, T.A. Badgwell, J.S. Qin, J.B. Rawlings, S.J. Wright, Nonlinear predictive control and moving horizon estimation – an introductory overview, in: P.M. Frank (Ed.), Advances in Control Highlights of ECC'99, Springer, London, 1999, pp. 391–449, http://dx.doi.org/10.1007/978-1-4471-0853-5_19.
[52] G. Guiochon, Preparative liquid chromatography, J. Chromatogr. A 965 (1–2) (2002) 129–161, http://dx.doi.org/10.1016/S0021-9673(01)01471-6.
[53] A. Seidel-Morgenstern, Experimental determination of single solute and competitive adsorption isotherms, J. Chromatogr. A 1037 (1–2) (2004) 255–272, http://dx.doi.org/10.1016/j.chroma.2003.11.108.
[54] N. Borg, K. Westerberg, A. Andersson, E. von Lieres, B. Nilsson, Effects of uncertainties in experimental conditions on the estimation of adsorption model parameters in preparative chromatography, Comput. Chem. Eng. 55 (0) (2013) 148–157, http://dx.doi.org/10.1016/j.compchemeng.2013.04.013.
[55] F. James, M. Sepúlveda, F. Charton, I. Quiñones, G. Guiochon, Determination of binary competitive equilibrium isotherms from the individual chromatographic band profiles, Chem. Eng. Sci. 54 (11) (1999) 1677–1696, http://dx.doi.org/10.1016/S0009-2509(98)00539-9.
[56] A. Felinger, A. Cavazzini, G. Guiochon, Numerical determination of the competitive isotherm of enantiomers, J. Chromatogr. A 986 (2) (2003) 207–225, http://dx.doi.org/10.1016/S0021-9673(02)01919-2.
[57] T. Hahn, A. Sommer, A. Osberghaus, V. Heuveline, J. Hubbuch, Adjoint-based estimation and optimization for column liquid chromatography models, Comput. Chem. Eng. 64 (0) (2014) 41–54, http://dx.doi.org/10.1016/j.compchemeng.2014.01.013.
[58] K. Johansson, S.S. Frederiksen, M. Degerman, M.P. Breil, J.M. Mollerup, B. Nilsson, Combined effects of potassium chloride and ethanol as mobile phase modulators on hydrophobic interaction and reversed-phase chromatography of three insulin variants, J. Chromatogr. A 1381 (0) (2015) 64–73, http://dx.doi.org/10.1016/j.chroma.2014.12.081.
[59] T.K. Sherwood, R.L. Pigford, C.R. Wilke, Mass Transfer, McGraw-Hill, New York, 1975.
[60] G. Carta, A. Jungbauer, Protein Chromatography: Process Development and Scale-Up, 1st ed., Wiley-VCH, Weinheim, 2010.
[61] J.M. Mollerup, Applied thermodynamics: a new frontier for biotechnology, Fluid Phase Equilib. 241 (1–2) (2006) 205–215, http://dx.doi.org/10.1016/j.fluid.2005.12.037.
[62] J.M. Mollerup, A Review of the thermodynamics of protein association to ligands, protein adsorption, and adsorption isotherms, Chem. Eng. Technol. 31 (6) (2008) 864–874, http://dx.doi.org/10.1002/ceat.200800082.
[63] T. Gu, Y.-H. Truei, G.-J. Tsai, G.T. Tsao, Modeling of gradient elution in multicomponent nonlinear chromatography, Chem. Eng. Sci. 47 (1) (1992) 253–262, http://dx.doi.org/10.1016/0009-2509(92)80219-3.
[64] C.A. Brooks, S.M. Cramer, Steric mass-action ion exchange: displacement profiles and induced salt gradients, AIChE J. 38 (12) (1992) 1969–1978, http://dx.doi.org/10.1002/aic.690381212.
[65] D. Karlsson, N. Jakobsson, A. Axelsson, B. Nilsson, Model-based optimization of a preparative ion-exchange step for antibody purification, J. Chromatogr. A 1055 (1–2) (2004) 29–39, http://dx.doi.org/10.1016/j.chroma.2004.08.151.
[66] P.K. Sweby, High resolution schemes using flux limiters for hyperbolic conservation laws, SIAM J. Numer. Anal. 21 (5) (1984) 995–1011, http://dx.doi.org/10.1137/0721062.
[67] B. van Leer, Towards the ultimate conservative difference scheme. V. A second-order sequel to Godunov's method, J. Comput. Phys. 32 (1) (1979) 101–136, http://dx.doi.org/10.1016/0021-9991(79)90145-1.
[68] A. Harten, High resolution schemes for hyperbolic conservation laws, J. Comput. Phys. 49 (3) (1983) 357–393, http://dx.doi.org/10.1016/0021-9991(83)90136-5.
[69] C. Shu, High order weighted essentially nonoscillatory schemes for convection dominated problems, Soc. Ind. Appl. Math. Rev. 51 (1) (2009) 82–126, http://dx.doi.org/10.1137/070679065.
[70] K. Sebastian, C.-W. Shu, Multidomain WENO finite difference method with interpolation at subdomain interfaces, J. Sci. Comput. 19 (1–3) (2003) 405–438, http://dx.doi.org/10.1023/A:1025372429380.
[71] X. Zhang, Y. Liu, C.-W. Shu, Maximum-principle-satisfying high order finite volume weighted essentially nonoscillatory schemes for convection-diffusion equations, J. Sci. Comput. 34 (2) (2012) A627–A658, http://dx.doi.org/10.1137/110839230.
[72] C.-S. Chou, C.-W. Shu, High order residual distribution conservative finite difference WENO schemes for convection-diffusion steady state problems on non-smooth meshes, J. Comput. Phys. 224 (2) (2007) 992–1020, http://dx.doi.org/10.1016/j.jcp.2006.11.006.
[73] A. Navarro, H. Caruel, L. Rigal, P. Phemius, Continuous chromatographic separation process: simulated moving bed allowing simultaneous withdrawal of three fractions, J. Chromatogr. A 770 (1–2) (1997) 39–50, http://dx.doi.org/10.1016/S0021-9673(96)01073-4.
[74] L. Aumann, G. Stroehlein, M. Morbidelli, Parametric study of a 6-column countercurrent solvent gradient purification (MCSGP) unit, Biotechnol. Bioeng. 98 (5) (2007) 1029–1042, http://dx.doi.org/10.1002/bit.21529.
[75] M. Behrens, P. Khobkhun, A. Potschka, S. Engell, Optimizing set point control of the MCSGP process, in: Control Conference (ECC), 2014 European, 2014, pp. 1139–1144, http://dx.doi.org/10.1109/ECC.2014.6862515.
[76] S. Engell, A. Toumi, Optimisation and control of chromatography, Comput. Chem. Eng. 29 (6) (2005) 1243–1252, http://dx.doi.org/10.1016/j.compchemeng.2005.02.034.
[77] J. Hakanen, Y. Kawajiri, K. Miettinen, L.T. Biegler, Interactive multi-objective optimization for simulated moving bed processes, Control Cybern. 36 (2) (2007) 230–282.
[78] F. Logist, J. Van Impe, Multi-objective dynamic optimisation of cyclic chemical reactors with distributed parameters, Chem. Eng. Sci. 80 (2012) 429–434, http://dx.doi.org/10.1016/j.ces.2012.06.040.
[79] L.T. Biegler, A.M. Cervantes, A. Wächter, Advances in simultaneous strategies for dynamic process optimization, Chem. Eng. Sci. 57 (4) (2002) 575–593, http://dx.doi.org/10.1016/S0009-2509(01)00376-1.
[80] J.T. Betts, Survey of numerical methods for trajectory optimization, J. Guid. Control Dyn. 21 (2) (1998) 193–207, http://dx.doi.org/10.2514/2.4231.
[81] J. Betts, Practical Methods for Optimal Control and Estimation Using Nonlinear Programming Advances in Design and Control, 2nd ed., Society for Industrial and Applied Mathematics, Philadelphia, PA, 2010.
[82] E. Hairer, G. Wanner, Solving ordinary differential equations ii: stiff and differential-algebraic problems, in: Springer Series in Computational Mathematics, 2nd ed., Springer-Verlag, Berlin, 1996.
[83] J. Åkesson, Optimica – an extension of modelica supporting dynamic optimization, in: 6th International Modelica Conference 2008, Modelica Association, 2008, pp. 57–66.
[84] J. Åkesson, K.-E. Årzén, M. Gäfvert, T. Bergdahl, H. Tummescheit, Modeling and optimization with Optimica and JModelica.org – languages and tools for solving large-scale dynamic optimization problems, Comput. Chem. Eng. 34 (11) (2010) 1737–1749, http://dx.doi.org/10.1016/j.compchemeng.2009.11.011.
[85] J. Andersson, A General-Purpose Software Framework for Dynamic Optimization (Ph.D. thesis), Arenberg Doctoral School, KU, Leuven, 2013.
[86] F. Magnusson, J. Åkesson, Dynamic optimization in jmodelica.org, Processes 3 (2) (2015) 471–496, http://dx.doi.org/10.3390/pr3020471.
[87] S.E. Magnusson, G. Söderlind, Index reduction in differential-algebraic equations using dummy derivatives, SIAM J. Sci. Comput. 14 (3) (1993) 677–692, http://dx.doi.org/10.1137/0914043.
[88] F.E. Cellier, E. Kofman, Continuous System Simulation, Springer, New York, NY, 2006.
[89] T. Blochwitz, M. Otter, M. Arnold, C. Bausch, C. Clau, H. Elmqvist, A. Junghanns, J. Mauss, M. Monteiro, T. Neidhold, D. Neumerkel, H. Olsson, J.-V. Peetz, S. Wolf, The Functional Mockup Interface for tool independent exchange of simulation models, in: Proceedings of the 8th International Modelica Conference, Dresden, Germany, 2011, pp. 105–114, http://dx.doi.org/10.3384/ecp11063105.
[90] C. Andersson, C. Führer, J. Åkesson, Assimulo: a unified framework for ODE solvers, Math. Comput. Simul. 116 (2015) 26–43, http://dx.doi.org/10.1016/j.matcom.2015.04.007.

[91] A.C. Hindmarsh, P.N. Brown, K.E. Grant, S.L. Lee, R. Serban, D.E. Shumaker, et al., SUNDIALS: suite of nonlinear and differential/algebraic equation solvers, ACM Trans. Math. Softw. 31 (3) (2005) 363–396, http://dx.doi.org/10.1145/1089014.1089020.
[92] B. Lennernäs, A CasADi Based Toolchain for JModelica.org (M.Sc. thesis), Lund University, Sweden, 2013.
[93] HSL, A Collection of Fortran Codes for Large Scale Scientific Computation, 2013 http://www.hsl.rl.ac.uk.
[94] A. Holmqvist, F. Magnusson, B. Nilsson, Dynamic multi-objective optimization of batch chromatographic separation processes, in: K.V. Gernaey, J.K. Huusom, R. Gani (Eds.), 12th International Symposium on Process Systems Engineering and 25th European Symposium on Computer Aided Process Engineering, Vol. 37 of Computer Aided Chemical Engineering, Elsevier, 2015, pp. 815–820, http://dx.doi.org/10.1016/B978-0-444-63578-5.50131-6.
[95] A. Ben-Tal, L. El Ghaoui, A. Nemirovski, in: I. Daubechies, E. Weinan, J.K. Lenstra, E. Süli (Eds.), Robust Optimization, Princeton Series in Applied Mathematics, Princeton University Press, 2009.
[96] A. Holmqvist, C. Andersson, F. Magnusson, J. Åkesson, Methods and tools for robust optimal control of batch chromatographic separation processes, Processes 3 (3) (2015) 568–606, http://dx.doi.org/10.3390/pr3030568.
[97] F. Logist, B. Houska, M. Diehl, J.F. Van Impe, Robust multi-objective optimal control of uncertain (bio)chemical processes, Chem. Eng. Sci. 66 (20) (2011) 4670–4682, http://dx.doi.org/10.1016/j.ces.2011.06.018.
[98] B. Houska, M. Diehl, Nonlinear robust optimization of uncertainty affine dynamic systems under the l-infinity norm, in: IEEE International Symposium on Computer-Aided Control System Design (CACSD), 2010, pp. 1091–1096, http://dx.doi.org/10.1109/CACSD.2010.5612793.
[99] B. Houska, F. Logist, J.V. Impe, M. Diehl, Robust optimization of nonlinear dynamic systems with application to a jacketed tubular reactor, J. Process Control 22 (6) (2012) 1152–1160, http://dx.doi.org/10.1016/j.jprocont.2012.03.008.
[100] Department of Health and Human Services U.S. Food and Drug Administration, Pharmaceutical cGMPs for the 21st Century: A Risk-Based Approach, Rockville, MD, USA, 2004.
[101] A. Chirino, A. Mire-Sluis, Characteristics biological products and assessing comparability following manufacturing changes, Nat. Biotechnol. 22 (11) (2004) 1383–1391, http://dx.doi.org/10.1038/nbt1030.
[102] A. Chanda, A.M. Daly, D.A. Foley, M.A. LaPack, S. Mukherjee, J.D. Orr, G.L. Reid, D.R. Thompson, H.W. Ward, Industry perspectives on process analytical technology: tools and applications in API development, Org. Process Res. Dev. 19 (1) (2015) 63–83, http://dx.doi.org/10.1021/op400358b.